

# Physical Layer Security Enhancement with Large Intelligent Surface-Assisted Networks

Jiayi Zhang, Hongyang Du, Derrick Wing Kwan Ng, *Senior Member, IEEE*, and  
Bo Ai, *Senior Member, IEEE*

## Abstract

Large intelligent surface (LIS)-aided wireless communications have drawn significant attention recently. We study the physical layer security of the downlink LIS-aided transmission framework for randomly located users in the presence of a multiple-antenna eavesdropper. To show the advantages of LIS-aided networks, we consider two practice scenarios: Communication with and without LIS. In both cases, we apply the stochastic geometry theory to derive exact probability density function (PDF) and cumulative distribution function (CDF) of signal-to-interference-plus-noise ratio. Furthermore, the obtained PDF and CDF are used to evaluate important security performance of wireless communication including the secrecy outage probability, the probability of nonzero secrecy capacity, and the average secrecy rate. In order to validate the accuracy of our analytical results, extensive Monte-Carlo simulations are subsequently conducted which provide interesting insights on how the secrecy performance is influenced by various important network parameters. Our results show that compared with the communication scenario without an LIS, the deployment of LIS can improve the performance and enhance the communication security substantially. In particular, the security performance of the system can be significantly improved by increasing the number of reflecting elements equipped in an LIS.

## Index Terms

Fisher-Snedecor  $\mathcal{F}$ -distribution, large intelligent surface, multiple-input multiple-output, stochastic geometry.

J. Zhang and H. Du are with the School of Electronic and Information Engineering, Beijing Jiaotong University, Beijing 100044, P. R. China. (e-mail: {jiayizhang, 17211140}@bjtu.edu.cn)

D. W. K. Ng is with the School of Electrical Engineering and Telecommunications, University of New South Wales, NSW 2052, Australia. (e-mail: w.k.ng@unsw.edu.au).

B. Ai is with the State Key Laboratory of Rail Traffic Control and Safety, Beijing Jiaotong University, Beijing 100044, China (e-mail: boai@bjtu.edu.cn).

## I. INTRODUCTION

Recently, large intelligent surface (LIS) has been proposed as a promising technique as it can achieve high spectral-/energy-efficiency through adaptively controlling the wireless signal propagation environment [1]. Specifically, LIS is a planar array which comprises a large number of nearly passive reflecting elements. By equipping the LIS with a controller, each element of the LIS can independently introduce a phase shift on the reflected signal. Besides, an LIS can be easily coated on existing infrastructures such as walls of buildings, facilitating low-cost and low-complexity implementation. By smartly adjusting the phase shifts induced by all the reflecting elements, the LIS has a lot of potential advantages such as enriching the channel by deliberately introducing more multi-paths, increasing the coverage area, or beamforming, while consuming very low amount of energy due to the passive nature of its elements. Recently, LIS has been introduced into many wireless communication systems. For instance, authors in [2] studied an LIS-assisted single-user multiple-input single-output (MISO) system and optimized the introduced phase shifts to maximize the total received signal power at the users. In [3], various designs were proposed for both the transmit power allocation at a base station (BS) and the phases introduced by the LIS elements to maximize the energy and the spectral efficiency of an LIS-assisted multi-user MISO system. Besides, the authors of [4] considered a downlink (DL) multiuser communication system where the signal-to-interference-plus noise ratio (SINR) was maximized for given phase shifts introduced by an LIS.

In practice, communication security is always a fundamental problem in wireless networks due to its broadcast nature. Besides traditional encryption methods adopted in the application layer, physical layer security [5]–[7] serves as an alternative for providing secure communication in fast access fifth-generation (5G) networks. Furthermore, physical layer security can achieve high-quality safety performance without requiring actual key distribution, which is a perfect match with the requirements of 5G. To fully exploit the advantages of 5G, multiple-antenna technology has become a powerful tool for enhancing the physical layer security in random wireless networks, e.g. [8]–[14]. In particular, with the degrees of freedom provided by multiple antennas, a transmitter can steer its beamforming direction to exploit the maximum directivity gain to reduce the potential of signal leakage to eavesdroppers. However, there are only a few works considering the physical layer security in the emerging LIS-based communication systems, despite its great importance for modern wireless systems. For example, an LIS-assisted secure communication system was investigated in [15], [16] but their communication systems only consist of a transmitter, one legitimate receiver, single eavesdropper, and an LIS with limited practical applications. Authors in [17]

studied a DL MISO broadcast system where a BS transmits independent data streams to multiple legitimate receivers and keeps them secret from multiple eavesdroppers. Besides, in order to conceive a practical LIS framework, user positions have to be taken into account using Stochastic Geometry (SG) for analyzing the system performance. In fact, SG is an efficient mathematical tool for capturing the topological randomness of networks [18], [19]. However, there are only a few works studying the impact of user-locations on the security performance.

Motivated by the aforementioned reasons, in this paper, we study the security performance of an LIS-aided DL multiple-input multiple-output (MIMO) system for randomly located roaming multiple-antenna users in the presence of a multiple-antenna eavesdropper. The main contributions of this paper are summarized as follows:

- We propose a novel LIS-aided MIMO framework exploiting the tools from SG to model the location of multiple-antenna users and a multiple-antenna eavesdropper. Besides, we adopt the blockage model and different path loss models to make our system more representative. We propose two approaches to simplify the performance analysis of LIS-aided paths: performing parameter transformation on the LoS paths, or applying the moment matching approximation proposed in [20, Theorem 3].
- We analyze two communication scenarios: LIS is adopted and it is not used. For each scenario, we derive the exact expressions of SINR and its probability density function (PDF) and cumulative distribution function (CDF) in closed-form expressions, respectively.
- We derive novel analytical expressions for characterizing the security performance metrics of the LIS-aided MIMO communication system, namely the secrecy outage probability (SOP), the probability of nonzero secrecy capacity (PNZ), and the average secrecy rate (ASR). The derived results can provide useful insights which is useful for communication system designers.

The remainder of the paper is organized as follows. In Section II, we introduce the system model of the LIS-aided DL MIMO communication system and derive the exact closed-form of PDF and CDF expressions of SINR for users and the eavesdropper. Section III formulates the security performance analysis in two scenarios and present the corresponding exact expressions of the performance. Section IV shows the simulation results and the accuracy of the obtained expressions is validated via Monte-Carlo simulations. Finally, Section V concludes this paper.

*Mathematical notations:* A list of mathematical symbols and functions most frequently used in this paper is available in Table I.

TABLE I  
MATHEMATICAL SYMBOLS AND FUNCTIONS

$v$	A subscript which denotes different users (the eavesdropper or the LIS). $v = u_1, \dots, u_M$ denotes the $M$ users respectively, $v = u_e$ is a eavesdropper and $v = u_l$ denotes the LIS.
$\sigma$	A subscript which denotes different links. $\sigma = 1$ denotes the LoS links between the BS and users (the eavesdropper), $\sigma = 2$ is the NLoS links between the BS and users (the eavesdropper), $\sigma = 3$ denotes the LoS link between the BS and the center of the LIS, $\sigma = 4$ denotes the LoS links between the center of the LIS and users (eavesdropper).
$\kappa$	A subscript which denotes different antennas.
$\mathbb{E}[\cdot]$	The mathematical expectation.
$r_2$	The radius of the disc.
$\alpha_L, C_L$	Path loss exponents for LoS link.
$\alpha_N, C_N$	Path loss exponents for NLoS link.
$\mathbf{H}^H$	Conjugate transpose.
$\mathbf{H}^T$	Transpose.
$\ \cdot\ _F$	The Frobenius norm.
$j$	$j = \sqrt{-1}$
$\{\Delta_i\}_{i=1}^L$	$\{\Delta_i\}_{i=1}^L$ denotes $\Delta_1, \Delta_2, \dots, \Delta_L$ .
$\Gamma(\cdot)$	Gamma function [21, eq. (8.310/1)]
$B(\cdot, \cdot)$	Beta function [21, Eq. (8.384.1)]
${}_2F_1(\cdot, \cdot; \cdot; \cdot)$	Gauss hypergeometric function [21, Eq. (9.111)]
$G_{p,q}^{m,n}(\cdot)$	Meijer's $G$ -function [21, eq. (9.301)]

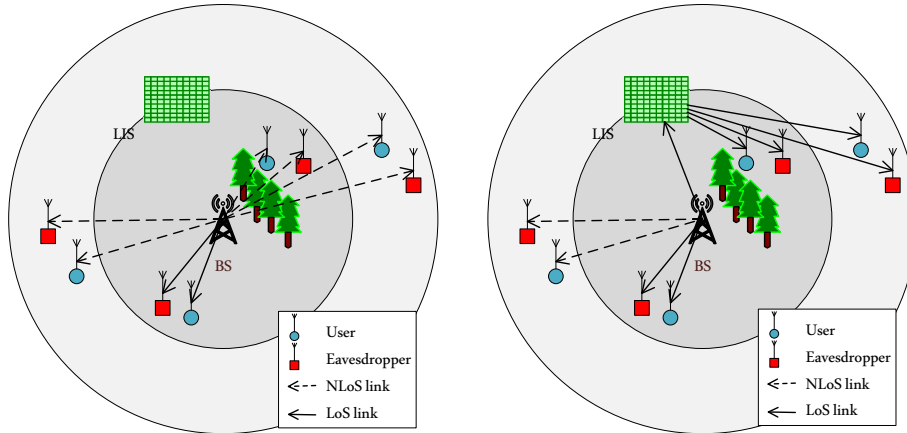


Fig. 1. Two practice scenarios: Communication without and with LIS.

## II. SYSTEM MODEL AND PRELIMINARIES

### A. System Description

Let us consider the DL MIMO-LIS system and assume that a BS equipped with  $M$  transmit antennas (TAs) communicates with  $M$  users each of which is equipped with  $K$  receive antennas (RAs). A LIS is installed between the BS and the users for assisting end-to-end communication. In addition, a malicious

eavesdropper<sup>1</sup> who equipped with  $K$  RAs aims to eavesdrop the information of the desired user. We assume that the number of rows is  $N$  and the number of columns is  $M$  for the LIS. Furthermore, the  $MN$  reflecting elements on the LIS serve  $M$  users simultaneously and the LIS is equipped with a controller to coordinate between the BS and the LIS for both channel acquisition and data transmission [2]. As such, the signal received from the BS can be manipulated by the LIS via adjusting the phase shifts and amplitude coefficients of the LIS elements.

Recently, a minimum mean squared error based channel estimation protocol has been proposed to estimate the LIS assisted links [22], and a novel three-phase pilot-based channel estimation framework was also proposed [23]. Thus, we can assume that the global channel state information (CSI) is perfectly known at the BS/LIS for their joint design of beamforming<sup>2</sup> [24]. Besides, the locations of the BS and the LIS are fixed, hence we assume that the distance between the BS and the LIS is known and denoted by  $d_{u_1,3}$ . In addition, the distances between the LIS and users are random and denoted by  $d_{\sigma,4}$ . Without loss of generality, we focus our attention on user  $m$ , where the distance between the LIS and user  $m$  is denoted by  $d_{u_m,4}$ . In particular, we assume that the users are located on a disc with a radius  $r_2$  according to homogeneous Poisson point processes (HPPP) [25] with density  $\lambda$  and the eavesdropper will try to choose a position that is close to the legitimate user.

In practice, the direct transmission link between the BS and the users may be blocked by trees or buildings. Such assumption is applicable for 5G and mmWave communication systems that are known to suffer from high path and penetration losses resulting in signal blockages. In order to show the benefits in adopting the LIS, we consider the following two practice communication scenarios:

- As shown in Fig. 1, in the first scenario, LIS is not adopted to enhancing the physical layer security and the quality of wireless communication. Specifically, the LoS links and NLoS links between the BS and users are all exist in our system.
- In the second case, when the LoS component between the BS and users is blocked, an LIS is deployed to leverage the LoS components with respect to both the BS and the users to assist their end-to-end communication of Fig. 1.

<sup>1</sup>Multiple-antenna technology can reduce the signal leakage to eavesdroppers [11], [12], [14], and wiretapping often caused by a eavesdropper who is close to the desired user.

<sup>2</sup>While acquiring the CSI of the eavesdropper is generally difficult, the results in this paper serve as theoretical performance upper bounds for the considered system. These bounds and the insights are still useful for wireless communication system designers when the CSI of the eavesdropper is not perfectly known.

### B. Blockage Model

A blockage model was proposed in [26], which can be regarded as an accurate approximation of the statistical blockage model [27] and incorporates the LoS ball model proposed in [28] as a special case. In the considered system model, we adopt the blockage model to divide the users process in the spherical region around the BS into two independent HPPPs: LoS users process and NLoS users process. In particular, we define  $q_L(r)$  as the probability that a link of length  $r$  is LoS. Each access link of separation  $r$  is assumed to be LoS with probability  $B_1$  if  $r \leq r_1$  and 0 otherwise:

$$q_L(r) = \begin{cases} B_1, & \text{if } r \leq r_1 \\ 0, & \text{otherwise} \end{cases}, \quad (1)$$

where  $0 \leq B_1 \leq 1$ . The parameter  $B_1$  can be interpreted as the average LoS area in the spherical region around the BS.

### C. User Location Model

Let us assume that the users are located according to a HPPP within the disc shown as Fig. 1. The PDF of the user locations have been derived as [29, eq. (30)]. As a result, the CDF of the user locations is given by

$$F_R(r) = \frac{r^2}{(r_2^2 - r_0^2)} - \frac{r_0^2}{(r_2^2 - r_0^2)}, \quad \text{if } r_0 < r < R. \quad (2)$$

where  $r_0$  is the minimum distance. Thus, the probability of the distance between the user and the BS is less than  $r_1$  can be expressed as

$$B_2 \triangleq \Pr(r \leq r_1) = F_R(r_1) = \frac{r_1^2}{(r_2^2 - r_0^2)} - \frac{r_0^2}{(r_2^2 - r_0^2)}. \quad (3)$$

### D. Path Loss Model

For the first communication scenario without an LIS, different path loss equations are applied to model the LoS and NLoS links as [26], [28]

$$L(d) = \begin{cases} C_1 d^{-\alpha_1}, & \text{if BS} \rightarrow \text{user link is LoS link} \\ C_2 d^{-\alpha_2}, & \text{if BS} \rightarrow \text{user link is NLoS link} \end{cases}, \quad (4)$$

where  $\alpha_1$  and  $\alpha_2$  are the LoS and NLoS path loss exponents, respectively,  $C_1 \triangleq 10^{-\frac{\beta_1}{10}}$  and  $C_2 \triangleq 10^{-\frac{\beta_2}{10}}$  can be regarded as the path loss intercepts of LoS and NLoS links at the reference distance. Typical values of  $\alpha_1$ ,  $\alpha_2$ ,  $\beta_1$ , and  $\beta_2$  are defined in [30, Table 1], while  $C_1 > C_2$  and  $\alpha_1 < \alpha_2$  hold in general.

For the second communication scenario with the assistance by the LIS, recently, the free-space path loss models of LIS-assisted wireless communications are developed for different situations in [31, Proposition 1]. Authors in [31] proposed that the free-space path loss of LIS-assisted communications is proportional to  $(d_1 d_2)^2$  in the far field case. Thus, we obtain

$$L(d_1, d_2) = C_{L_1} C_{L_2} d_1^{-2} d_2^{-2}. \quad (5)$$

### E. Small-Scale Fading

In order to conceive a practical LIS framework, we assume that the small-scale fading of each link follows independent but not identically distributed (i.n.i.d.) Fisher-Snedecor  $\mathcal{F}$  fading distributions<sup>3</sup> [32] and the fading parameters of different links is defined as  $\mathbf{Q}_{v,\sigma}$ . For the first communication scenario, in order to characterize the LoS and NLoS links between the BS and users (eavesdropper), the small-scale fading matrices are defined as

$$\mathbf{Q}_{v,\sigma} = \begin{bmatrix} q_{1,1}^{v,\sigma} & \cdots & q_{1,M}^{v,\sigma} \\ \vdots & \vdots & \vdots \\ q_{K,1}^{v,\sigma} & \cdots & q_{K,M}^{v,\sigma} \end{bmatrix}, \quad (6)$$

where  $\mathbf{Q}_{v,\sigma}$  ( $\sigma = 1, 2$ ) is a  $K \times M$  matrix. Letting  $v = u_m$ , we obtain the small-scale fading matrix between the BS and user  $m$ . Using [32, Eq. (5)], the PDF of the elements of (6) can be expressed as

$$f_X(x) = \frac{2m^m ((m_s - 1)\Omega)^{m_s}}{B(m, m_s)} \frac{x^{2m-1}}{(mr^2 + (m_s - 1)\Omega)^{m+m_s}}, \quad (7)$$

where  $\Omega = \mathbb{E}[r^2]$  is the mean power,  $m$  and  $m_s$  are physical parameters which represent the fading severity and shadowing parameters, respectively. For the second case, the small-scale fading matrices for

<sup>3</sup>In the literature, authors in [29] conceived a LIS-aided MIMO framework using Nakagami- $m$  distribution. However, Fisher-Snedecor  $\mathcal{F}$  distribution is more general and includes the case of Nakagami- $m$  distribution as  $m_s \rightarrow \infty$  and its subsequent special cases, such as Rayleigh ( $m = 1$ ) and one-sided Gaussian ( $m = 1/2$ ). In addition, we consider the weak correlation scenario, i.e., the BS communicates with the user using RIS in the far-field region. By using Fisher-Snedecor  $\mathcal{F}$  fading distribution, we can take shadowing caused by the user-positions into account [7] which conceive a more practical LIS framework.

the LoS links between the BS and users (eavesdropper) are same as the first case. In addition, in order to model the LoS links between the BS and the LIS, the small-scale fading matrix is defined as

$$\mathbf{Q}_{u_l,3} = \begin{bmatrix} q_{1,1}^{u_l,3} & \cdots & q_{1,M}^{u_l,3} \\ \vdots & \vdots & \vdots \\ q_{MN,1}^{u_l,3} & \cdots & q_{MN,M}^{u_l,3} \end{bmatrix}, \quad (8)$$

where  $\mathbf{Q}_{u_l,3}$  is a  $MN \times M$  matrix.

In order to model the LoS links between the LIS and users (eavesdropper), the small-scale fading matrixes are defined as

$$\mathbf{Q}_{v,4} = \begin{bmatrix} q_{1,1}^{v,4} & \cdots & q_{1,MN}^{v,4} \\ \vdots & \vdots & \vdots \\ q_{K,1}^{v,4} & \cdots & q_{K,MN}^{v,4} \end{bmatrix}, \quad (9)$$

where  $\mathbf{Q}_{v,4}$  is a  $K \times MN$  matrix. Letting  $v = u_m$ , we get the small-scale fading matrix between the LISs and user  $m$ .

### F. Directional Beamforming

Highly directional beamforming antenna arrays are deployed at the BS to compensate the significant path-loss in the considered system. For mathematical tractability and similar to [26], [27], the antenna pattern of users can be approximated by a sectored antenna model in [33] which is given by

$$G_{v,\kappa}(\theta) = \begin{cases} G_{v,\kappa}, & \text{if } |\theta| \leq \theta_c \\ g_{v,\kappa}, & \text{otherwise,} \end{cases} \quad (10)$$

where  $\theta$ , distributed in  $[0, 2\pi]$ , is the angle between the BS and the user,  $\theta_c$  denotes the beamwidth of the main lobe, for each TA,  $G_{v,\kappa}$  and  $g_{v,\kappa}$  are respectively the array gains of main and sidelobes. In practice, the BS can adjust their antennas according to the CSI and the directivity gain of users is  $G_{v,\kappa}$ . In the following, we denote the boresight direction of the antennas as  $0^\circ$ . For simplifying the performance analysis, different antennas of the authorized users and the malicious eavesdropper are assumed to have same array gains<sup>4</sup>. Thus, without loss of generality, we assume that  $G_{v,\kappa} = G_v$  ( $\kappa = 1, \dots, K$ ) and  $g_{v,\kappa} = g_v$ .

<sup>4</sup>This assumption is just for simplifying the performance analysis. However, the obtained analysis methods can be extended to the different array gains cases by adopting (10) correspondingly.

### G. SINR Analysis in Two Communication Scenarios

Let us consider a composite channel model of large-scale and small-scale fading. It is assumed that the distance  $d_{v,\sigma}$ ,  $v = u_1, \dots, u_M, u_e$  and  $\sigma = 1, 2, 3, 4$  are i.n.i.d. and the large-scale fading is represented by the path loss. In the DL transmission, the BS sends the following  $M \times 1$  information bearing vector:

$$\mathbf{s} = \left[ s_{v_1}, \dots, s_{v_M} \right]^T, \quad (11)$$

where  $s_{v_m}$  denotes the signal intended for user  $m$ .

In the first communication scenario, there are LoS and NLoS links. The signal received by user  $m$  or the eavesdropper from the BS can be expressed as

$$y_\sigma^\chi = \sqrt{G_\chi} \mathbf{Q}_{\chi,\sigma} \mathbf{P} \mathbf{s} \sqrt{L(d_{\chi,\sigma})} + N_0, \quad (12)$$

where  $\chi = u_m, u_e$ , ( $\sigma = 1, 2$ ),  $\mathbf{P} \triangleq [\mathbf{p}_{u_1}, \mathbf{p}_{u_2}, \dots, \mathbf{p}_{u_M}]$  is the active beamforming weight at the BS, and  $N_0$  denotes the additive white Gaussian noise, which is modeled as a realization of a zero-mean complex circularly symmetric Gaussian variable with variance  $\sigma_N^2$ .

In the second communication scenario, there are LoS and LIS-aided links. For LoS links, the signal received by the user or the eavesdropper can be obtained by letting  $\sigma = 1$  in (12). For LIS-aided links, the signal can be expressed as

$$y_{\text{LIS}}^\chi = \sqrt{G_\chi} \mathbf{Q}_{\chi,4} \mathbf{\Phi} \mathbf{Q}_3 \mathbf{P} \mathbf{s} \sqrt{L(d_3, d_{\chi,4})} + N_0, \quad (13)$$

where  $\mathbf{\Phi} \triangleq \text{diag}[\beta_1 \phi_1, \beta_2 \phi_2, \dots, \beta_{MN} \phi_{MN}]$  is a diagonal matrix accounting for the effective phase shift introduced by all the elements of the LIS,  $\beta_n \in (0, 1]$  represents the amplitude reflection coefficient,  $\phi_n = \exp(j\theta_n)$ ,  $n = 1, \dots, MN$ ,  $\theta_n \in [0, 2\pi)$  denotes the phase shift.

The SINRs involved in the first case and the second case can be obtained using the design of passive beamforming process proposed in [29]. For the first case, the received SINR at user  $m$  and the eavesdropper are denoted as  $\text{SINR}_{\chi,\sigma}$ , and it can be expressed as

$$\text{SINR}_{\chi,\sigma} = \frac{\mathcal{G}_\chi C_\sigma \left\| \hat{\mathbf{h}}_{\chi,\sigma} \right\|_F^2 (d_{\chi,\sigma})^{-\alpha_\sigma} p_{u_m}}{\beta_{\max}^2 Q^2 \sigma_N^2}, \quad (14)$$

where  $\mathcal{G}_{u_m} \triangleq G_{u_m}$ ,  $\mathcal{G}_{u_e} \triangleq G_{u_e}(\theta)$ ,  $Q \triangleq K - M - 1$ , and  $\beta_{\max}$  is obtained by finding the maximum

amplitude coefficient,  $p_{u_m}$  denotes the transmit power of the BS for user  $m$  and

$$\hat{\mathbf{h}}_{\chi,\sigma} = \begin{bmatrix} q_{1,1}^{\chi,\sigma} & \cdots & q_{1,M}^{\chi,\sigma} \\ \vdots & \vdots & \vdots \\ q_{Q,1}^{\chi,\sigma} & \cdots & q_{Q,M}^{\chi,\sigma} \end{bmatrix} \quad (15)$$

is a  $Q \times M$  matrix which denotes the channel gain of user  $m$ . In addition,  $\sigma = 1$  denotes that the path between the BS and the user is LoS and  $\sigma = 2$  means that the path is NLoS. We can see that the eavesdropper's SINR is affected by the random directivity gain  $G_{u_e}(\theta)$ .

For the second case, the SINR of LoS path can be obtained by letting  $\sigma = 1$  in (14). For the LIS-aided path, with the help of the design of passive beamforming process [29], the SINR with the optimal phase shift design of LIS's reflector array<sup>5</sup> can be derived as  $\text{SINR}_{\chi,\text{LIS}}$ ,  $\chi = u_m, u_e, \sigma = 1, 2$

$$\text{SINR}_{\chi,\text{LIS}} = \frac{\mathcal{G}_\chi C_{L_1} C_{L_2} \left\| \hat{\mathbf{h}}_{\chi,\text{LIS}} \right\|_F^2 (d_3 d_{\chi,4})^{-2} p_{u_m}}{\beta_{\max}^2 Q^2 \sigma_N^2}, \quad (16)$$

where

$$\hat{\mathbf{h}}_{\chi,\text{LIS}} = \begin{bmatrix} (q_{1,1}^{\chi,4}) \cdot (q_{1,m}^{u,3}) & \cdots & (q_{1,MN}^{\chi,4}) \cdot (q_{MN,m}^{u,3}) \\ \vdots & \vdots & \vdots \\ (q_{Q,1}^{\chi,4}) \cdot (q_{1,m}^{u,3}) & \cdots & (q_{Q,MN}^{\chi,4}) \cdot (q_{MN,m}^{u,3}) \end{bmatrix} \quad (17)$$

is a  $Q \times MN$  matrix.

With the help of (14) and (16), we derive the exact PDF and CDF expressions for each scenario's SINR in terms of multivariate Fox's  $H$ -function [37, eq. (A-1)], which are summarized in the following Theorems.

**Theorem 1.** *In the first communication scenario, let  $Z_{\chi,\sigma} = \text{SINR}_{\chi,\sigma}$ , the CDF of  $Z_{\chi,\sigma}$  is expressed as*

$$F_{Z_{\chi,\sigma}}(z) = \prod_{\ell=1}^{QM} \frac{1}{\Gamma(m_{s_\ell}) \Gamma(m_\ell)} (H_{\text{CDF}_{1,2}} - H_{\text{CDF}_{1,0}}), \quad (18)$$

<sup>5</sup>Many methods have been proposed to obtain the optimal effective phase shift introduced by all the elements of the LIS [2], [34]–[36]. For example, using a novel and simple method that is based on binary search tree algorithm [36], we can maximize the instantaneous SINR to obtain (16) without the CSI.

where

$$H_{\text{CDF}_{1,h}} \triangleq H_{1,2;2,1;\dots;2,1}^{0,1;1,2;\dots;1,2} \left( \begin{array}{c} \frac{A_1 z r_h^{\alpha\sigma} m_1}{\bar{\gamma}_1 (m_{s_1} - 1)} \\ \vdots \\ \frac{A_1 z r_h^{\alpha\sigma} m_{Q_M}}{\bar{\gamma}_{Q_M} (m_{s_{Q_M}} - 1)} \end{array} \left| \begin{array}{l} \left(1 - \frac{2}{\alpha\sigma}; 1, \dots, 1\right) : (1, 1), (1 - m_{s_1}, 1); \dots; (1, 1), (1 - m_{s_{Q_M}}, 1) \\ (0; 1, \dots, 1) \left(-\frac{2}{\alpha\sigma}; 1, \dots, 1\right) : (m_1, 1); \dots; (m_{Q_M}, 1) \end{array} \right. \right) \times \frac{2r_h^2}{(r_2^2 - r_0^2) \alpha\sigma} \quad (\bar{h} = 0, 2), \quad (19)$$

$$A_1 = \frac{\mathcal{G}_x C_\sigma p_{um}}{\beta_{\max}^2} Q^2 \sigma_N^2, \quad \{m_\ell\}_{i=1}^{Q_M} = \left\{ \left\{ m_{q,n}^{\chi,\sigma} \right\}_{n=1}^M \right\}_{q=1}^Q, \quad \{m_{s_\ell}\}_{i=1}^{Q_M} = \left\{ \left\{ m_{s_{q,n}}^{\chi,\sigma} \right\}_{n=1}^M \right\}_{q=1}^Q, \quad \text{and } \{\Omega_\ell\}_{i=1}^{Q_M} = \left\{ \left\{ \Omega_{q,n}^{\chi,\sigma} \right\}_{n=1}^M \right\}_{q=1}^Q.$$

*Proof:* Please refer to Appendix A. ■

**Theorem 2.** In the first communication scenario, the PDF of the SINR for the user  $m$  and eavesdropper can be given by

$$f_{Z_{\chi,\sigma}}(z) = \prod_{\ell=1}^{Q_M} \frac{1}{\Gamma(m_{s_\ell}) \Gamma(m_\ell)} (H_{\text{PDF}_{1,2}} - H_{\text{PDF}_{1,0}}), \quad (20)$$

where

$$H_{\text{PDF}_{1,h}} \triangleq H_{1,2;2,1;\dots;2,1}^{0,1;1,2;\dots;1,2} \left( \begin{array}{c} \frac{A_1 z r_h^{\alpha} m_1}{\bar{\gamma}_1 (m_{s_1} - 1)} \\ \vdots \\ \frac{A_1 z r_h^{\alpha} m_{Q_M}}{\bar{\gamma}_{Q_M} (m_{s_{Q_M}} - 1)} \end{array} \left| \begin{array}{l} \left(-\frac{2}{\alpha}; 1, \dots, 1\right) : (1, 1), (1 - m_{s_1}, 1); \dots; (1, 1), (1 - m_{s_{Q_M}}, 1) \\ (1; 1, \dots, 1) \left(-1 - \frac{2}{\alpha}; 1, \dots, 1\right) : (m_1, 1); \dots; (m_{Q_M}, 1) \end{array} \right. \right) \times \frac{2r_h^{2+\alpha}}{(r_2^2 - r_0^2) \alpha} A_1 \quad (\bar{h} = 0, 2). \quad (21)$$

*Proof:* Following similar procedures as in Appendix B, we can derive the PDF of  $Z_{\chi,\sigma}$  by calculating

$$f_Y(y) = \int_{r_0^{\alpha\sigma}}^{r_2^{\alpha\sigma}} x f_X(xy) f_D(x) dx, \quad (22)$$

where  $f_X(\cdot)$  is given as [38, eq. (23)] and  $f_D(\cdot)$  has been derived as (A-4). ■

Then, we focus on the derivation for the performance metric in the second scenario.

**Theorem 3.** In the second communication scenario, let  $Z_{\chi,\text{LIS}} = \text{SINR}_{\chi,\text{LIS}}$ , the CDF of  $Z_{\chi,\text{LIS}}$  can be

expressed as

$$F_{Z_{\chi,\text{LIS}}}(z) = \prod_{\ell=1}^{QMN} \frac{1}{\prod_{i=1}^2 \Gamma(m_{s_i,\ell}) \Gamma(m_{i,\ell})} (H_{\text{CDF}_{2,2}} - H_{\text{CDF}_{2,0}}), \quad (23)$$

where

$$H_{\text{CDF}_{2,\hbar}} \triangleq H_{1,2:2,1;\dots;1,2}^{0,1:1,2;\dots;1,2} \left( \Delta \left| \begin{array}{l} (0; 1, \dots, 1) : (1, 1), \{(1 - m_{s_{i,1}}, 1)\}_{i=1}^2; \dots; (1, 1), \{(1 - m_{s_{i,QMN}}, 1)\}_{i=1}^2 \\ (0; 1, \dots, 1) (-\frac{2}{2}; 1, \dots, 1) : \{(m_{i,1}, 1)\}_{i=1}^2; \dots; \{(m_{i,QMN}, 1)\}_{i=1}^2 \end{array} \right. \right) \\ \times \frac{r_{\hbar}^2}{(r_2^2 - r_0^2)} \quad (\hbar = 0, 2), \quad (24)$$

$$\Delta = \left( \frac{A_2 z r_2^2 m_{1,1} m_{2,1}}{\prod_{i=1}^2 (m_{s_{i,1}} - 1) \bar{\gamma}_1}, \dots, \frac{A_2 z r_2^2 m_{1,QMN} m_{2,QMN}}{\prod_{i=1}^2 (m_{s_{i,QMN}} - 1) \bar{\gamma}_{QMN}} \right)^{\mathbf{T}}, \quad A_2 = \frac{g_{\chi} C_{L_1} C_{L_2} (d_3)^{-2} p_{u_m}}{\beta_{\max}^2} Q^2 \sigma_N^2, \quad \{m_{1,\ell}\}_{i=1}^{QMN} = \left\{ \left\{ m_{q,n}^{\chi,4} \right\}_{n=1}^M \right\}_{q=1}^Q, \\ \{m_{1,s_{\ell}}\}_{i=1}^{QMN} = \left\{ \left\{ m_{s_{q,n}}^{\chi,4} \right\}_{n=1}^M \right\}_{q=1}^Q, \quad \{\Omega_{1,\ell}\}_{i=1}^{QMN} = \left\{ \left\{ \Omega_{q,n}^{\chi,4} \right\}_{n=1}^M \right\}_{q=1}^Q, \quad \{m_{2,\ell}\}_{i=1}^{MN} = \{m_{n,m}^{u_i,3}\}_{n=1}^{MN}, \quad \{m_{2,s_{\ell}}\}_{i=1}^{MN} = \\ \{m_{s_{n,m}}^{u_i,3}\}_{n=1}^{MN}, \quad \text{and} \quad \{\Omega_{2,\ell}\}_{i=1}^{MN} = \{\Omega_{n,m}^{u_i,3}\}_{n=1}^{MN}.$$

*Proof:* Please refer to Appendix B. ■

**Theorem 4.** In the second communication scenario, the PDF of  $Z_{\chi,\text{LIS}}$  can be deduced as

$$f_{Z_{\chi,\text{LIS}}}(z) = \prod_{\ell=1}^{QMN} \frac{1}{\prod_{i=1}^2 \Gamma(m_{s_i,\ell}) \Gamma(m_{i,\ell})} (H_{\text{PDF}_{2,2}} - H_{\text{PDF}_{2,0}}), \quad (25)$$

where

$$H_{\text{PDF}_{2,\hbar}} \triangleq H_{1,2:2,1;\dots;1,2}^{0,1:1,2;\dots;1,2} \left( \Delta \left| \begin{array}{l} (-1; 1, \dots, 1) : (1, 1), \{(1 - m_{s_{i,1}}, 1)\}_{i=1}^2; \dots; (1, 1), \{(1 - m_{s_{i,QMN}}, 1)\}_{i=1}^2 \\ (1; 1, \dots, 1) (-2; 1, \dots, 1) : \{(m_{i,1}, 1)\}_{i=1}^2; \dots; \{(m_{i,QMN}, 1)\}_{i=1}^2 \end{array} \right. \right) \\ \times \frac{r_{\hbar}^4}{(r_2^2 - r_0^2)} A_2 \quad (\hbar = 0, 2), \quad (26)$$

*Proof:* Following similar procedures as in Appendix B, we can express the PDF of  $Z_{\chi,\text{LIS}}$  with the help of (22). ■

**Remark 1.** By comparing Theorem 1 and Theorem 3 or Theorem 2 and Theorem 4, we can see that, caused by the characteristics of Fisher-Snedecor  $\mathcal{F}$  distribution, the CDF and PDF of the SINR for the LIS-aided path are very similar to that of the LoS or NLoS path. This insight is very useful because we only need to further investigate Theorem 1 and Theorem 2 for performance analysis of the first communication

scenario. In other words, we can get the results for the LIS-assisted scenario through simple parameter transformation. Specifically, we can let  $m_\ell \rightarrow m_{1,\ell}m_{2,\ell}$ ,  $m_{s_\ell} \rightarrow m_{s_{1,\ell}}m_{s_{2,\ell}}$ ,  $\Gamma(m_\ell) \rightarrow \Gamma(m_{1,\ell})\Gamma(m_{2,\ell})$ ,  $\Gamma(m_{s_\ell}) \rightarrow \Gamma(m_{s_{1,\ell}})\Gamma(m_{s_{2,\ell}})$ ,  $(m_\ell) \rightarrow (m_{1,\ell});(m_{2,\ell})$ ,  $(m_{s_\ell}) \rightarrow (m_{s_{1,\ell}});(m_{s_{2,\ell}})$ ,  $QM \rightarrow QMN$  and  $\alpha_\sigma = 2$ , where  $A \rightarrow B$  means replacing  $A$  with  $B$ , and the results for the LIS-aided scenario will follow.

**Remark 2.** An accurate closed-form approximation to the distribution of a sum of Fisher-Snedecor  $\mathcal{F}$  RVs using a single Fisher-Snedecor  $\mathcal{F}$  RV was presented in [20, Theorem 3]. Thus, with the help of Remark 1 and [20, Theorem 3], Theorems 1-4 can be re-derived from a single Fisher-Snedecor  $\mathcal{F}$  distribution to simplify calculations. In addition, the physical layer security over the Fisher-Snedecor  $F$  wiretap fading channels has been studied in [39]. Considering our HPPP model, the results of performance analysis can also be transformed easily.

### III. SECURITY PERFORMANCE ANALYSIS

The secrecy rate over fading wiretap channels [40] is defined as the difference between the main channel rate and the wiretap channel rate as

$$C_s(Z_{u_m,\sigma}, Z_{u_e,\sigma}) = \begin{cases} C_{u_m,\sigma} - C_2, & Z_{u_m,\sigma} > Z_{u_e,\sigma} \\ 0, & \text{otherwise} \end{cases} = \begin{cases} \log_2\left(\frac{1+Z_{u_m,\sigma}}{1+Z_{u_e,\sigma}}\right), & Z_{u_m,\sigma} > Z_{u_e,\sigma} \\ 0, & \text{otherwise} \end{cases}, \quad (27)$$

which means that a positive secrecy rate can be assured if and only if the received SINR at user  $m$  has a superior quality than that at the eavesdropper.

In the considered LIS assisted system, we assume that the location of users are random and define

$$\mathbf{P}_A \triangleq [P_{LoS}, P_{NLoS}] \quad (28)$$

and

$$\mathbf{P}_B \triangleq [Pr_{LoS}Pr_G, Pr_{LoS}Pr_g, Pr_{NLoS}Pr_G, Pr_{NLoS}Pr_g], \quad (29)$$

where  $Pr_{LoS} \triangleq B_1B_2$ ,  $Pr_{NLoS} \triangleq 1 - B_1B_2$ ,  $Pr_G \triangleq \frac{\theta_c}{180}$ ,  $Pr_g \triangleq 1 - \frac{\theta_c}{180}$ ,  $P_{LoS}$  represents the probability that the path is LoS in two scenarios,  $P_{NLoS}$  denotes the probability that the path is NLoS in the first scenario or LIS-assisted in the second scenario,  $P_G$  is the probability that the eavesdropper's directivity gain is the same as the user's and  $P_g$  represents the probability that the eavesdropper's directional gain is  $\mathbf{g}_{u_e}$ . Besides, we assume that the eavesdropper has the same path loss as user  $m$  because they are close to each other.

### A. Outage Probability (OP) Characterization

The OP is defined as the probability that the instantaneous SINR is less than a predetermined threshold  $Z_{\text{th}}$ . In the first communication scenario, the OP can be directly calculated as

$$OP = \mathbf{P}_A [F_{Z_{u_m,1}}(Z_{\text{th}}), F_{Z_{u_m,2}}(Z_{\text{th}})]^T, \quad (30)$$

which can be evaluated directly with the help of (18).

**Remark 3.** *In the second communication scenario, the OP can be obtained by replacing  $F_{Z_{u_m,2}}(Z_{\text{th}})$  in (30) with  $F_{Z_{u_m,4}}(Z_{\text{th}})$ . We can observe that OP decreases when the channel condition of user  $m$  is improved. Besides, a LIS equipped with more reflecting elements will also make the OP lower.*

### B. SOP Characterization

The secrecy outage probability (SOP), is defined as the probability that the instantaneous secrecy capacity falls below a target secrecy rate threshold. In the first communication scenario, the SOP can be written as

$$SOP = \mathbf{P}_B \begin{bmatrix} \Pr(Z_{u_m,1} \leq R_s Z_{u_e,1,G} + R_s - 1) \\ \Pr(Z_{u_m,1} \leq R_s Z_{u_e,1,g} + R_s - 1) \\ \Pr(Z_{u_m,2} \leq R_s Z_{u_e,2,G} + R_s - 1) \\ \Pr(Z_{u_m,2} \leq R_s Z_{u_e,2,g} + R_s - 1) \end{bmatrix} = \mathbf{P}_B [SOP_{1,G}, SOP_{1,g}, SOP_{2,G}, SOP_{2,G}]^T, \quad (31)$$

where  $R_s = 2^{R_t}$ ,  $Z_{u_e,1,G}$  denotes that the eavesdropper's directional gain is  $G_{u_e}$  and  $Z_{u_e,1,g}$  denotes that the eavesdropper's directional gain is  $g_{u_e}$ . With the help of (31) and Theorems 1-4, we derive the following propositions.

**Proposition 1.** *Let  $SOP_{\sigma,\lambda} \triangleq \Pr(Z_{u_m,\sigma} \leq R_s Z_{u_e,\sigma,\lambda} + R_s - 1)$  denotes the element of the matrix in (31) and we can express  $SOP_{\sigma,\lambda}$  as*

$$SOP_{\sigma,\lambda} = \mathcal{S}_{2,2} - \mathcal{S}_{2,0} - \mathcal{S}_{0,2} + \mathcal{S}_{0,0}, \quad (32)$$

where  $\mathcal{S}_{p,q}$  ( $p = 0, 2$  and  $q = 0, 2$ ) can be written as

$$\mathcal{S}_{p,q} = \frac{4A_1 r_p^2 r_q^{2+\alpha\sigma}}{\alpha_{u_m} \alpha_{u_e} (r_2^2 - r_0^2)^2} \times H_{4,4;2,1;\dots;2,1;0,1}^{0,3;1,2;\dots;1,2;1,0} \left( H_{SOP} \left| \begin{array}{l} H_{S_1} : (1, 1), (1 - m_{s_1}, 1); \dots; (1, 1), (1 - m_{s_{2QM}}, 1); - \\ H_{S_2} : (m_1, 1); \dots; (m_{2QM}, 1); (0, 1) \end{array} \right. \right), \quad (33)$$

$$H_{SOP} \triangleq \left( \frac{A_1 z r_p^\alpha m_1}{\bar{\gamma}_1 (m_{s_1} - 1)}, \dots, \frac{A_1 z r_q^\alpha m_{2QM+1}}{\bar{\gamma}_{2QM+1} (m_{s_{2QM+1}} - 1)}, e \right)^T,$$

$$H_{S_1} \triangleq \left( 1 - \frac{2}{\alpha}; \underbrace{1, \dots, 1}_{QM}, \underbrace{0, \dots, 0}_{QM}, 0 \right); \left( -\frac{2}{\alpha}; \underbrace{0, \dots, 0}_{QM}, \underbrace{1, \dots, 1}_{QM}, 0 \right); \left( 2, \underbrace{-1, \dots, -1}_{2QM+1} \right); \left( 0, \underbrace{1, \dots, 1}_{2QM+1} \right),$$

$$H_{S_2} \triangleq \left( 0; \underbrace{1, \dots, 1}_{QM}, \underbrace{0, \dots, 0}_{QM}, 0 \right) \left( -\frac{2}{\alpha}; \underbrace{1, \dots, 1}_{QM}, \underbrace{0, \dots, 0}_{QM}, 0 \right); \left( 1; \underbrace{0, \dots, 0}_{QM}, \underbrace{1, \dots, 1}_{QM}, 0 \right); \left( -1 - \frac{2}{\alpha}; \underbrace{0, \dots, 0}_{QM}, \underbrace{1, \dots, 1}_{QM}, 0 \right)$$

and  $e$  is a positive number close to zero (e.g.,  $e = 10^{-6}$ ).

*Proof:*  $SOP_{\sigma,\lambda}$  can be expressed as

$$SOP_{\sigma,\lambda} = \int_0^\infty F_{Z_{u_m,\sigma}}(R_s Z + R_s - 1) f_{Z_{u_e,\sigma,\lambda}}(Z) dZ, \quad (34)$$

substituting (18) and (20) into (34), yields

$$SOP_{\sigma,\lambda} = \prod_{\ell_1=1}^{QM} \frac{1}{\Gamma(m_{u_m, s_{\ell_1}}) \Gamma(m_{u_m, \ell_1})} \prod_{\ell_2=1}^{QM} \frac{1}{\Gamma(m_{u_e, s_{\ell_2}}) \Gamma(m_{u_e, \ell_2})}$$

$$\times \int_0^\infty (H_{u_m, CDF_{1,2}} - H_{u_m, CDF_{1,0}}) (H_{u_e, PDF_{1,2}} - H_{u_e, PDF_{1,0}}) dZ$$

$$\triangleq \mathcal{S}_{2,2} - \mathcal{S}_{2,0} - \mathcal{S}_{0,2} + \mathcal{S}_{0,0}. \quad (35)$$

Substituting (19) and (21) into  $\mathcal{S}_{p,q}$  and changing the order of integration, the Integral part in  $\mathcal{S}_{p,q}$  can be expressed as

$$I_1 = \int_0^\infty (R_s Z + R_s - 1)^{\sum_{\ell_1=1}^{QM} \zeta_{u_m, \ell_1}} Z^{\sum_{\ell_2=1}^{QM} \zeta_{u_e, \ell_2}} dZ. \quad (36)$$

Let  $t = \frac{R_s}{R_s - 1} Z$ ,  $I_1$  can be written as after some algebraic manipulations

$$I_1 = (R_s - 1)^{\sum_{\ell_1=1}^{QM} \zeta_{u_m, \ell_1}} \left( \frac{R_s - 1}{R_s} \right)^{1 + \sum_{\ell_2=1}^{QM} \zeta_{u_e, \ell_2}} \underbrace{\int_0^\infty (t + 1)^{\sum_{\ell_1=1}^{QM} \zeta_{u_m, \ell_1}} (t)^{\sum_{\ell_2=1}^{QM} \zeta_{u_e, \ell_2}} dt}_{I_2}, \quad (37)$$

let  $\mathcal{L}\{p(t)\} = P(x)$ . Using the property of Laplace transform, we have

$$\mathcal{L}\left\{\int_0^t p(z)dz\right\} = \frac{P(x)}{x}. \quad (38)$$

According to the final value theorem, it follows that

$$\lim_{t \rightarrow \infty} \left(\int_0^t p(z)dz\right) = e \frac{P(e)}{e} = P(e). \quad (39)$$

With the help of (39) and [37, eq. (2.9.6)],  $I_2$  can be solved as

$$\begin{aligned} I_2 &= \mathcal{L}\left\{(t+1)^{\sum_{\ell_1=1}^{QM} \zeta_{u_m, \ell_1}} (t)^{\sum_{\ell_2=1}^{QM} \zeta_{u_e, \ell_2}}\right\} \\ &= \Gamma\left(1 + \sum_{\ell_2=1}^{QM} \zeta_{u_e, \ell_2}\right) \Psi\left(1 + \sum_{\ell_2=1}^{QM} \zeta_{u_e, \ell_2}, 2 + \sum_{\ell_1=1}^{QM} \zeta_{u_m, \ell_1} + \sum_{\ell_2=1}^{QM} \zeta_{u_e, \ell_2}, s\right), \end{aligned} \quad (40)$$

where  $\Psi(\cdot)$  is the tricomi confluent hypergeometric function [21, eq. (9.210.2)]. Using [41, eq. (07.33.07.0003.01)] and letting  $\{t_\ell\}_{\ell=1}^{2QM+1} = \left\{\{\zeta_{u_m, \ell_1}\}_{\ell_1=1}^{QM}, \{\zeta_{u_e, \ell_2}\}_{\ell_2=1}^{QM}, s\right\}$ , (40) and (37), we can derive  $S_{2,2}$  as (32) to complete the proof. ■

**Remark 4.** In the second communication scenario, the SOP of the LIS-aided path can be obtained with the help of Theorem 1. From (32), we can see that the SOP will decrease when the fading parameter  $m_{u_m}$  and  $m_{s_{u_m}}$  increase because of better communication conditions. In addition, we can see that  $Q$ ,  $M$ , and  $N$  will affect the dimension of the multivariate Fox's  $H$ -function, so  $Q$ ,  $M$  and  $N$  have a greater impact on the SOP than the channel parameters. Thus, it is obvious that communication system designers can increase  $N$  of LIS for lower SOP.

### C. PNZ Characterization

Another fundamental performance metric of the PLS is the probability of non-zero secrecy capacity (PNZ) which can be defined as

$$PNZ = \mathbf{P}_B \begin{bmatrix} \Pr(Z_{u_m,1} > Z_{u_e,1,G}) \\ \Pr(Z_{u_m,1} > Z_{u_e,1,g}) \\ \Pr(Z_{u_m,2} > Z_{u_e,2,G}) \\ \Pr(Z_{u_m,2} > Z_{u_e,2,g}) \end{bmatrix} = \mathbf{P}_B [PNZ_{1,G}, PNZ_{1,g}, PNZ_{2,G}, PNZ_{2,g}]^T. \quad (41)$$

Thus, we exploit (41) and Theorems 1-4 to arrive the following proportions.

**Proposition 2.** Let  $PNZ_{\sigma,\lambda} \triangleq \Pr(Z_{u_m,\sigma} > R_s Z_{u_e,\sigma,\lambda})$  denotes the element of the matrix in (41) and we can express  $PNZ_{\sigma,\lambda}$  as

$$PNZ_{\sigma,\lambda} = \mathcal{P}_{2,2} - \mathcal{P}_{2,0} - \mathcal{P}_{0,2} + \mathcal{P}_{0,0}, \quad (42)$$

where  $\mathcal{P}_{p,q}$  ( $p = 0, 2$  and  $q = 0, 2$ ) can be written as

$$\mathcal{P}_{p,q} = \frac{4A_1 r_p^{2} r_q^{2+\alpha\sigma}}{e\alpha_{u_m} \alpha_{u_e} (r_2^2 - r_0^2)^2} \times H_{3,4;2,1;\dots;2,1}^{0,3;1,2;\dots;1,2} \left( H_{PNZ} \left| \begin{array}{l} H_{S_1} : (1, 1), (1 - m_{s_1}, 1); \dots; (1, 1), (1 - m_{s_{2QM}}, 1) \\ H_{S_2} : (m_1, 1); \dots; (m_{2QM}, 1) \end{array} \right. \right), \quad (43)$$

$$H_{PNZ} \triangleq \left( \frac{A_1 z r_p^\alpha m_1}{e\tilde{\gamma}_1 (m_{s_1}-1)}, \dots, \frac{A_1 z r_q^\alpha m_{2QM}}{e\tilde{\gamma}_{2QM} (m_{s_{2QM}}-1)} \right)^\top, \quad H_{P_1} = \left( 1 - \frac{2}{\alpha}; \underbrace{1, \dots, 1}_{QM}, \underbrace{0, \dots, 0}_{QM} \right); \left( -\frac{2}{\alpha}; \underbrace{0, \dots, 0}_{QM}, \underbrace{1, \dots, 1}_{QM} \right); \left( 0, \underbrace{1, \dots, 1}_{2QM} \right),$$

$$H_{P_2} \triangleq \left( 0; \underbrace{1, \dots, 1}_{QM}, \underbrace{0, \dots, 0}_{QM} \right) \left( -\frac{2}{\alpha}; \underbrace{1, \dots, 1}_{QM}, \underbrace{0, \dots, 0}_{QM} \right); \left( 1; \underbrace{0, \dots, 0}_{QM}, \underbrace{1, \dots, 1}_{QM} \right); \left( -1 - \frac{2}{\alpha}; \underbrace{0, \dots, 0}_{QM}, \underbrace{1, \dots, 1}_{QM} \right).$$

*Proof:*  $PNZ_{\sigma,\lambda}$  is defined as

$$PNZ_{\sigma,\lambda} = \int_0^\infty F_{Z_{u_e,\sigma}}(Z) f_{Z_{u_m,\sigma}}(Z) dZ, \quad (44)$$

substituting (18) and (20) into (44), we obtain that

$$PNZ_{\sigma,\lambda} = \prod_{\ell_1=1}^{QM} \frac{1}{\Gamma(m_{u_m, s_{\ell_1}}) \Gamma(m_{u_m, \ell_1})} \prod_{\ell_2=1}^{QM} \frac{1}{\Gamma(m_{u_e, s_{\ell_2}}) \Gamma(m_{u_e, \ell_2})} \times \int_0^\infty (H_{u_m, CDF_{1,2}} - H_{u_m, CDF_{1,0}}) (H_{u_e, PDF_{1,2}} - H_{u_e, PDF_{1,0}}) dZ$$

$$\triangleq \mathcal{P}_{2,2} - \mathcal{P}_{2,0} - \mathcal{P}_{0,2} + \mathcal{P}_{0,0}. \quad (45)$$

By changing the order of integration, we can express the integral part of  $\mathcal{P}_{p,q}$  as

$$I_3 = \int_0^\infty Z^{\sum_{\ell_1=1}^{QM} \zeta_{u_m, \ell_1} + \sum_{\ell_2=1}^{QM} \zeta_{u_e, \ell_2} + 1} dZ, \quad (46)$$

which can be solved using the final value theorem as [20, eq. (34)]. Thus, (42) is obtained, which completes the proof.  $\blacksquare$

**Remark 5.** In the second communication scenario, the PNZ of the LIS-aided path can be easily obtained according to Theorem 1. From (42), we can see that PNZ will increase when user  $m$  has good commu-

nication conditions or when the eavesdropper is in a bad communication environment. Besides, we can observe that PNZ is also more susceptible to  $Q$ ,  $M$ , and  $N$ , because these parameters directly determine the dimension of the multivariate Fox's  $H$ -function. In general, system designers can improve PNZ by increasing the size of the LIS.

#### D. ASR Characterization

The ASR describes the difference between the rate of the main channel and wiretap channel over instantaneous SINR can be expressed as

$$ASR = \mathbf{P}_B \begin{bmatrix} E [C_s (Z_{u_m,1}, Z_{u_e,1,G})] \\ E [C_s (Z_{u_m,1}, Z_{u_e,1,g})] \\ E [C_s (Z_{u_m,2}, Z_{u_e,2,G})] \\ E [C_s (Z_{u_m,2}, Z_{u_e,2,g})] \end{bmatrix} = \mathbf{P}_B [ASC_{1,G}, ASC_{1,g}, ASC_{2,G}, ASC_{2,g}]^T. \quad (47)$$

We derive the following proposition using (47) and Theorems 1-4.

**Proposition 3.** We assume that  $ASR_{\sigma,\lambda} = E [C_s (Z_{u_m,\sigma}, Z_{u_e,\sigma,\lambda})]$  is the element of the matrix in (47) and we can expressed  $ASR_{\sigma,\lambda}$  as

$$ASR_{\sigma,\lambda} = \sum_{i=1}^2 (\mathcal{A}_{2,2,i} - \mathcal{A}_{2,0,i} - \mathcal{A}_{0,2,i} + \mathcal{A}_{0,0,i}) - (\mathcal{A}_{2,2,3} - \mathcal{A}_{2,0,3} - \mathcal{A}_{0,2,3} + \mathcal{A}_{0,0,3}), \quad (48)$$

where  $\mathcal{A}_{p,q,i}$  ( $p = 0, 2$ ,  $q = 0, 2$  and  $i = 1, 2$ ) can be derived as

$$\mathcal{A}_{p,q,i} = \frac{4A_1 r_p^{2q} r_q^{2+\alpha\sigma}}{e \ln 2 \alpha_{u_m} \alpha_{u_e} (r_2^2 - r_0^2)^2} \times H_{5,4;2,1;\dots;2,1,0,1}^{0,4;1,2;\dots;1,2,1,0} \left( H_{ASR} \left| \begin{array}{l} H_{A_1} : (1, 1), (1 - m_{s_1}, 1); \dots; (1, 1), (1 - m_{s_{2QM}}, 1); - \\ H_{A_2} : (m_1, 1); \dots; (m_{2QM}, 1); (1, 1) \end{array} \right. \right), \quad (49)$$

$$H_{ASR} \triangleq \left( \frac{A_1 z r_p^\alpha m_1}{\bar{\gamma}_1 (m_{s_1} - 1)}, \dots, \frac{A_1 z r_q^\alpha m_{2QM+1}}{\bar{\gamma}_{2QM+1} (m_{s_{2QM+1}} - 1)}, e \right)^T,$$

$$H_{A_1} \triangleq \left( 1 - \frac{2}{\alpha}; \underbrace{1, \dots, 1}_{QM}, \underbrace{0, \dots, 0}_{QM}, 0 \right); \left( -\frac{2}{\alpha}; \underbrace{0, \dots, 0}_{QM}, \underbrace{1, \dots, 1}_{QM}, 0 \right); \left( 1, \underbrace{-1, \dots, -1}_{QM}, \underbrace{1, \dots, 1}_{QM}, 0 \right); \left( 0, \underbrace{1, \dots, 1}_{2QM}, 0 \right),$$

$$H_{A_2} \triangleq \left( 0; \underbrace{1, \dots, 1}_{QM}, \underbrace{0, \dots, 0}_{QM+1} \right); \left( -\frac{2}{\alpha}; \underbrace{1, \dots, 1}_{QM}, \underbrace{0, \dots, 0}_{QM+1} \right); \left( 1; \underbrace{0, \dots, 0}_{QM}, \underbrace{1, \dots, 1}_{QM} \right); \left( -1 - \frac{2}{\alpha}; \underbrace{0, \dots, 0}_{QM}, \underbrace{1, \dots, 1}_{QM}, 0 \right),$$

and  $\mathcal{A}_{p,q,3}$  ( $p = 0, 2$  and  $q = 0, 2$ ) can be expressed as

$$\mathcal{A}_{p,q,i} \triangleq \frac{2A_1 r_q^{2+\alpha_\sigma}}{e \ln 2 \alpha_{ue} (r_2^2 - r_0^2)} \times H_{4,2:2,1;\dots;2,1;0,1}^{0,3:1,2;\dots;1,2;1,0} \left( H_{ASC_2} \left| \begin{array}{l} H_{A_{1,2}} : (1, 1), (1 - m_{s_1}, 1); \dots; (1, 1), (1 - m_{s_{QM}}, 1); - \\ H_{A_{2,2}} : (m_1, 1); \dots; (m_{QM}, 1); (1, 1) \end{array} \right. \right), \quad (50)$$

$$H_{ASC_2} \triangleq \left( \frac{A_1 z r_p^\alpha m_1}{\bar{\gamma}_1 (m_{s_1} - 1)}, \dots, \frac{A_1 z r_q^\alpha m_{QM+1}}{\bar{\gamma}_{QM+1} (m_{s_{QM+1}} - 1)}, e \right)^\top, H_{A_{1,2}} \triangleq \left( -\frac{2}{\alpha}; \underbrace{0, \dots, 0}_{QM}, 0 \right); \left( \underbrace{1, 1, \dots, 1}_{QM}, 0 \right); \left( \underbrace{0, 1, \dots, 1}_{QM}, 0 \right)$$

and  $H_{A_{2,2}} \triangleq \left( \underbrace{0; 1, \dots, 1}_{QM}, 0 \right); \left( \underbrace{1; 1, \dots, 1}_{QM}, 0 \right); \left( -1 - \frac{2}{\alpha}; \underbrace{1, \dots, 1}_{QM}, 0 \right).$

*Proof:*  $ASC_{\sigma,\lambda}$  can be expressed as

$$ASC_{\sigma,\lambda} = \sum_{i=1}^2 \mathcal{I}_{\sigma,\lambda,i} - \mathcal{I}_{\sigma,\lambda,3} = \sum_{i=1}^2 (\mathcal{A}_{2,2,i} - \mathcal{A}_{2,0,i} - \mathcal{A}_{0,2,i} + \mathcal{A}_{0,0,i}) - (\mathcal{A}_{2,2,3} - \mathcal{A}_{2,0,3} - \mathcal{A}_{0,2,3} + \mathcal{A}_{0,0,3}), \quad (51)$$

where

$$\begin{cases} \mathcal{I}_{\sigma,\lambda,1} = \int_0^\infty \log_2(1+Z) f_{Z_{u_m,\sigma}}(Z) F_{Z_{u_e,\sigma}}(Z) dZ, \\ \mathcal{I}_{\sigma,\lambda,2} = \int_0^\infty \log_2(1+Z) f_{Z_{u_e,\sigma}}(Z) F_{Z_{u_m,\sigma}}(Z) dZ, \\ \mathcal{I}_{\sigma,\lambda,3} = \int_0^\infty \log_2(1+Z) f_{Z_{u_e,\sigma}}(Z) dZ \end{cases} \quad (52)$$

and

$$\begin{aligned} ASR_{\sigma,\lambda,i} &= \prod_{\ell_1=1}^{QM} \frac{1}{\Gamma(m_{u_m,s_{\ell_1}}) \Gamma(m_{u_m,\ell_1})} \prod_{\ell_2=1}^{QM} \frac{1}{\Gamma(m_{u_e,s_{\ell_2}}) \Gamma(m_{u_e,\ell_2})} \\ &\quad \times \int_0^\infty \log_2(1+Z) (H_{u_m,CDF_{1,2}} - H_{u_m,CDF_{1,0}}) (H_{u_e,PDF_{1,2}} - H_{u_e,PDF_{1,0}}) dZ \\ &\triangleq \mathcal{A}_{2,2,i} - \mathcal{A}_{2,0,i} - \mathcal{A}_{0,2,i} + \mathcal{A}_{0,0,i}. \end{aligned} \quad (53)$$

Substituting (18) and (20) into (52), we can express the integral part of  $\mathcal{I}_{\sigma,\lambda,i}$  ( $i = 1, 2$ ) as

$$I_4 = \int_0^\infty \log_2(Z+1) Z^{\sum_{\ell_1=1}^{QM} \zeta_{u_m,\ell_1} + \sum_{\ell_2=1}^{QM} \zeta_{u_e,\ell_2}} dZ, \quad (54)$$

which has been solved using the final value theorem as [20, eq. (49)]. Thus,  $I_3$  can be written as

$$I_4 = \frac{1}{e \ln 2} \int_S \frac{\Gamma(1-s) \Gamma^2 \left( -\sum_{\ell_1=1}^{QM} \zeta_{u_m, \ell_1} + \sum_{\ell_2=1}^{QM} \zeta_{u_e, \ell_2} \right) \Gamma \left( 1 + \sum_{\ell_1=1}^{QM} \zeta_{u_m, \ell_1} + \sum_{\ell_2=1}^{QM} \zeta_{u_e, \ell_2} \right)}{\Gamma \left( 1 - \sum_{\ell_1=1}^{QM} \zeta_{u_m, \ell_1} - \sum_{\ell_2=1}^{QM} \zeta_{u_e, \ell_2} \right)} e^s ds. \quad (55)$$

With the help of (52), we obtain  $\mathcal{I}_{\sigma, \lambda, i}$  ( $i = 1, 2$ ). Similarly, following the same methodology, one can easily derive  $\mathcal{I}_{\sigma, \lambda, 3}$ . The proof is now completed.  $\blacksquare$

**Remark 6.** For second communication scenario, the ASR of the LIS-aided path can also be obtained according to Theorem 1. From (48), as expected, better channel conditions will result in a higher ASR. In addition, we can also observe that the ASR can be improved by assuring larger LIS because the multivariate Fox's  $H$ -function in ASR is also more easily affected by  $Q$ ,  $M$ , and  $N$  as SOP and PNZ.

#### IV. NUMERICAL RESULTS

In this section, analytical results are presented to illustrate the advantages of applying the LIS to enhance the security of the DL MIMO communication system. We assume that the noise variances  $\sigma_N$  at user  $m$  and the eavesdropper are identical and  $\sigma_N = 0$  dB. The transmit power  $p_{u_m}$  is defined in dB with respect to the noise variance. The array gains of main and sidelobes are set to  $G = 30$  dB and  $g = -10$  dB. For the small scale fading, we set  $m_{u_m} = 5$ ,  $m_{u_e} = 3$ ,  $m_{s_{u_m}} = 5$ ,  $m_{s_{u_e}} = 3$ ,  $\bar{\gamma}_{u_m} = \bar{\gamma}_{u_e} = -10$  dB. The path loss exponent is set to  $\alpha_1 = 2$ ,  $C_{L_1} = C_{L_2} = C_1 = 10$  and  $C_2 = 8$ . Moreover, in the considered simulation scenario, we assume that  $r_2 = 400$ ,  $r_1 = 300$ ,  $r_0 = 1$ ,  $\beta_{\max} = 1$ ,  $d_3 = 30$  and  $B_1 = 0.3$ . The numerical results are verified via Monte Carlo simulations by averaging the obtain performance over  $10^6$  realizations.

Figure 2 depicts the OP performance versus transmit power  $p_{u_m}$  with  $R_{\text{th}} = 1$ ,  $K = 4$ ,  $M = 2$ ,  $Z_{\text{th}} = 0$  dB. As it can be observed, the OP decreases as transmit power and  $N$  increase, which means that the introduction of an LIS can provide better communication for the considered MIMO wireless communication system. In addition, when  $\alpha_2 = 2.5$ , we can see that LIS can not improve the system performance when the number of reflecting elements in LIS is small. This is because the system outage probability is mainly affected by the path loss. When the signal is sent directly to the user, the signal propagation distance is shorter. In addition, we can observe that when the path loss of NLoS is large, for example, when  $\alpha_2 = 3$ , the performance gain brought by LIS is significant. Furthermore, analytical

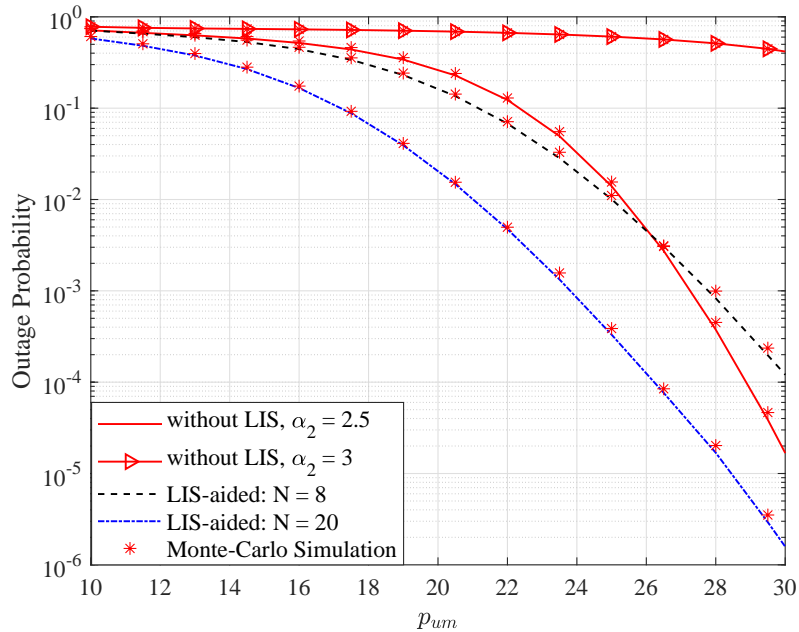


Fig. 2. Outage probability versus the transmit power for user  $m$ .

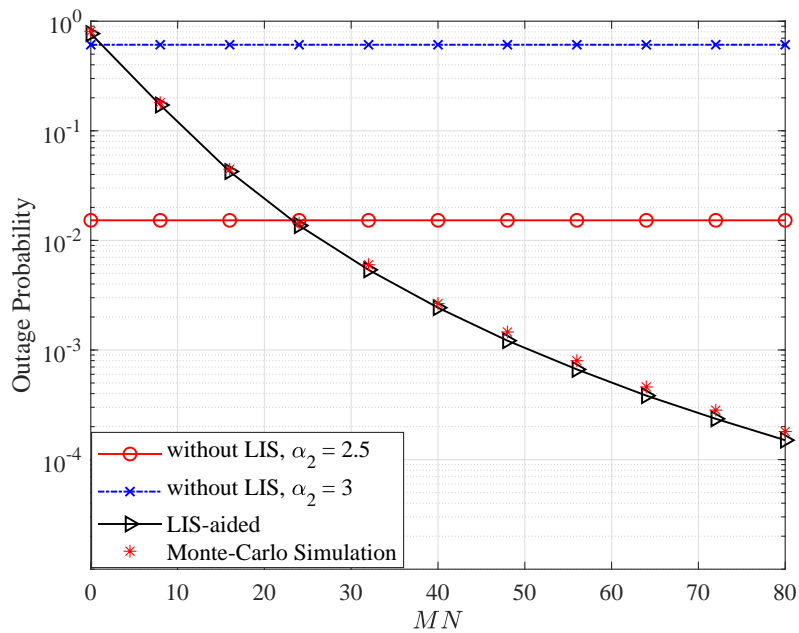


Fig. 3. Outage probability versus the number of reflecting elements equipped in LIS.

results perfectly match with the Monte Carlo simulations confirming the accuracy of the derived analytical results, as can be seen in the figure.

Figure 3 illustrates the OP performance versus the number of reflecting elements equipped in LIS, with  $R_{th} = 1$ ,  $K = 4$ ,  $M = 2$ ,  $Z_{th} = 0$  dB, and  $p_{um} = 25$  dB. From Fig. 3, we can observe that

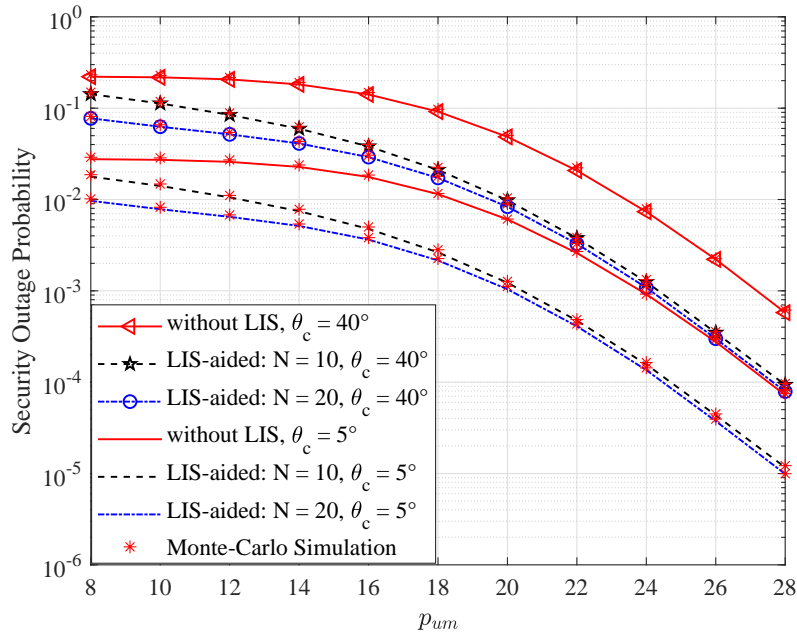


Fig. 4. Security outage probability versus the transmit power for user  $m$ .

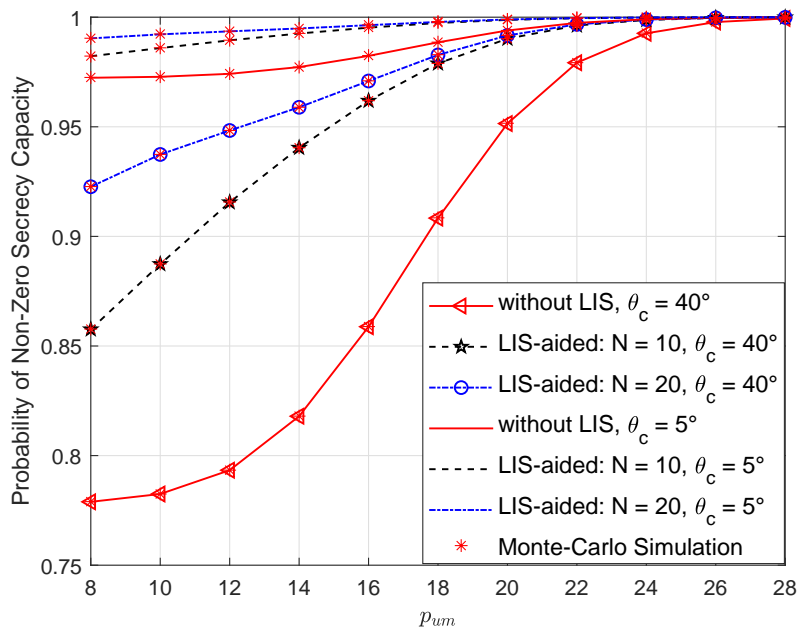


Fig. 5. Probability of non-zero secrecy capacity versus transmit power for user  $m$ .

the OP decreases as  $N$  increases, which means that the setting of LIS can significantly improving the performance of wireless communication system especially when the path loss is large. Furthermore, when  $N$  is sufficiently large such that the reflected signal power by the LIS dominates the total received power at the user  $m$ , we can observe that there is a diminishing slope in the OP. Thus, to achieve a low OP

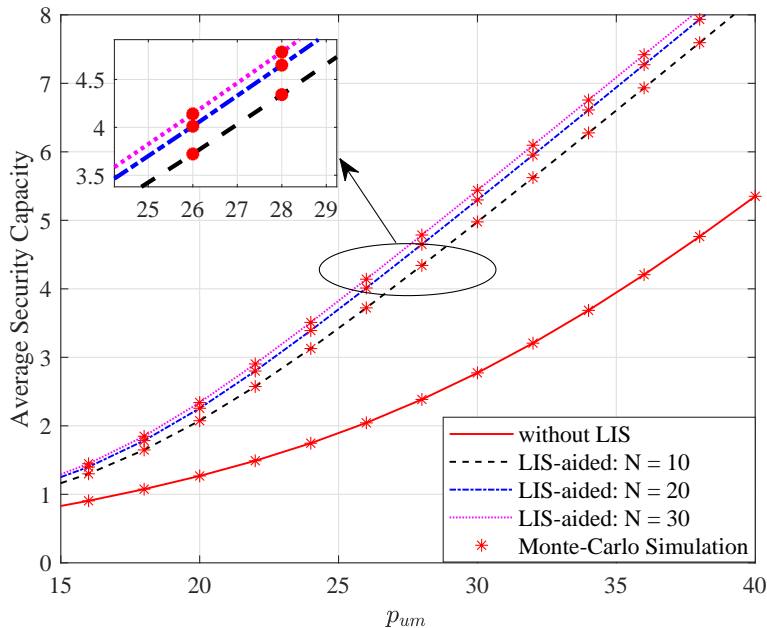


Fig. 6. Average security rate versus transmit power for user  $m$ .

at the user, there exists a trade-off between the number of reflecting elements in LIS and the transmit power of BS.

Figure 4 depicts the SOP performance versus transmit power  $p_{u_m}$  under different  $\theta_c$  with  $R_{th} = 1$ ,  $K = 4$ ,  $M = 2$ ,  $Z_{th} = 0$  dB, and  $\alpha_2 = 3$ . For a certain setting of the parameters, the SOP decreases as the transmit power of the BS increases. Besides, it can be easily observed that the SOP increases as  $\theta_c$  decreases. This is because large value of  $\theta_c$  offers the eavesdroppers a higher possibility of exploiting the larger array gains. Again, it is evident that the analytical results match the Monte Carlo simulations well.

Figure 5 shows the analytical and simulated PNZ versus transmit power  $p_{u_m}$  under different  $\theta_c$  with  $R_{th} = 1$ ,  $K = 4$ ,  $M = 2$ ,  $Z_{th} = 0$  dB, and  $\alpha_2 = 3$ . As it can be observed, the PNZ decreases as  $\theta_c$  increases because the eavesdropper is more likely to receive signals. Moreover, similar to the results in Fig. 4, the use of LIS can enhance the security of the system. Furthermore, notice that the signal propagation distance is longer when the LIS is used. Thus, if the transmit signal power is not high or the amount of reflecting elements on the LIS is not large, the performance gain brought by LIS is limited. However, with the increase of transmit power, the communication scenario with LIS enjoys a better security performance.

Figure 6 illustrates the ASR as a function of the transmit power  $p_{u_m}$  for different settings of  $N$  with  $K = 4$ ,  $M = 2$ , and  $\alpha_2 = 3$ . As expected, there is a perfect match between our analytical and simulated results. Like SOP and PNZ, when the transmit power is not large, there is only a small difference for

the ASR between communication with LIS and without LIS. This is also because adopting LIS increases the signal propagation distance. In contrast, when the power is moderate to high, LIS is very useful for enhancing the security of the physical layer, and as analyzed in Remark 6, the larger the  $N$  is, the more obvious the performance gain is. Furthermore, it can be observed that there is a diminishing return in the ASR gain due to increasing  $N$ . This is because when  $N$  is large, the security performance of the system is mainly limited by other factors, such as the channel quality and the path loss.

## V. CONCLUSION

We proposed a new LIS-aided secure communication system and presented the exact of expressions for CDF and PDF of the SINR for both cases of the LIS is used or not used. Our analytical framework showed the analytical performance expressions of LIS-aided communication subsume the counterpart case without exploiting LIS which can be obtained by some simple parameter transformation of the former case. Secrecy metrics, including the SOP, PNZ, and ASR, were all derived with closed-form expressions in terms of the multivariate Fox's  $H$ -function. Numerical results confirmed that the LIS can bring significant performance gains and enhance the security of the proposed communication system, in particular, by increasing the amount of reflecting elements. In addition, the accuracy of our analytical results were efficiently validated by Monte-Carlo simulation results.

## APPENDIX A

### PROOF OF THEOREM 1

Based on the result derived in (14) and exploiting the fact that the elements of  $\mathbf{Q}_{v,\sigma}$  are i.n.i.d., the effective channel gain vector of user  $m$  (eavesdropper) can be transformed into

$$\left\| \widehat{\mathbf{h}}_{\chi,\sigma} \right\|_F^2 = \sum_{q=1}^Q \sum_{n=1}^M |q_{q,n}^{\chi,\sigma}|^2 \quad (\text{A-1})$$

Note that the elements of  $\mathbf{Q}_{v,\sigma}$  obey the Fisher-Snedecor  $\mathcal{F}$  distribution with fading parameters  $m_\ell^{\chi,\sigma}$ ,  $m_{s_\ell}^{\chi,\sigma}$  and  $\Omega_\ell^{\chi,\sigma}$ . For the sake of presentation, we define  $\{q_\ell\}_{i=1}^{QM} = \left\{ \{q_{q,n}\chi, \sigma\}_{n=1}^M \right\}_{q=1}^Q$ .

Letting  $\gamma_\ell = \bar{\gamma}_\ell |q_\ell|^2 / \Omega_\ell$ , where  $\bar{\gamma}_\ell = \mathbb{E}[\Omega_\ell]$ , we have

$$f_\gamma(\gamma_\ell) = \frac{m_\ell^{m_\ell} \cdot ((m_{s_\ell} - 1) \bar{\gamma}_\ell)^{m_{s_\ell}} \gamma_\ell^{m_\ell - 1}}{B(m_\ell, m_{s_\ell}) (m_\ell \gamma_\ell + (m_{s_\ell} - 1) \bar{\gamma}_\ell)^{m_\ell + m_{s_\ell}}}. \quad (\text{A-2})$$

Thus, let  $X = \sum_{\ell=1}^{QM} \gamma_{\ell}$ , the CDF of  $X$  is obtained with the help of [38, eq. (23)] and [37, eq (A.1)] as

$$F_X(x) = \prod_{\ell=1}^{QM} \frac{1}{\Gamma(m_{s_{\ell}}) \Gamma(m_{\ell})} \int_{\mathcal{L}_1} \int_{\mathcal{L}_2} \cdots \int_{\mathcal{L}_{QM}} \left( \frac{1}{2\pi j} \right)^{QM} \frac{1}{\Gamma\left(1 + \sum_{\ell=1}^{QM} \zeta_{\ell}\right)} \\ \times \prod_{\ell=1}^{QM} \Gamma(m_{\ell} - \zeta_{\ell}) \Gamma(\zeta_{\ell}) \Gamma(m_{s_{\ell}} + \zeta_{\ell}) \left( \frac{x m_{\ell}}{\bar{\gamma}_{\ell} (m_{s_{\ell}} - 1)} \right)^{\zeta_{\ell}} d\zeta_1 d\zeta_2 \cdots d\zeta_{QM}. \quad (\text{A-3})$$

Let  $D = (d_{u,m,\sigma})^{-\alpha_{\sigma}}$ , hence, using [29, eq. (30)], we derive the PDF of  $D$  as

$$f_D(d) = \frac{2}{(r_2^2 - r_0^2) \alpha_{\sigma}} d^{\frac{2}{\alpha_{\sigma}} - 1}, \quad \text{if } r_0^{\alpha_{\sigma}} < d < r_2^{\alpha_{\sigma}}. \quad (\text{A-4})$$

Let us define  $Y = X/D$ , because  $X$  and  $D$  are statistically independent, the CDF of  $Y$  can be formulated as

$$F_Y(y) = P\{Y \leq y\} = P\{X \leq yD\} = \int_{r_0^{\alpha_{\sigma}}}^{r_2^{\alpha_{\sigma}}} F_X(xy) f_D(x) dx. \quad (\text{A-5})$$

Then, by replacing (A-3) and (A-4) into (A-5) and exchanging the order of integration according to Fubini's theorem, we get

$$F_Y(y) = \frac{2}{(r_2^2 - r_0^2) \alpha_{\sigma}} \prod_{\ell=1}^{QM} \frac{1}{\Gamma(m_{s_{\ell}}) \Gamma(m_{\ell})} \left( \frac{1}{2\pi j} \right)^{QM} \int_{\mathcal{L}_1} \int_{\mathcal{L}_2} \cdots \int_{\mathcal{L}_{QM}} \frac{1}{\Gamma\left(1 + \sum_{\ell=1}^{QM} \zeta_{\ell}\right)} \\ \times \prod_{\ell=1}^{QM} \Gamma(m_{\ell} - \zeta_{\ell}) \Gamma(\zeta_{\ell}) \Gamma(m_{s_{\ell}} + \zeta_{\ell}) \left( \frac{y m_{\ell}}{\bar{\gamma}_{\ell} (m_{s_{\ell}} - 1)} \right)^{\zeta_{\ell}} \underbrace{\int_{r_0^{\alpha_{\sigma}}}^{r_2^{\alpha_{\sigma}}} x^{\sum_{\ell=1}^{QM} \zeta_{\ell} + \frac{2}{\alpha_{\sigma}} - 1} dx}_{I_A} d\zeta_1 d\zeta_2 \cdots d\zeta_{QM}. \quad (\text{A-6})$$

$I_A$  can easily be deduced. Letting  $Z = A_1 Y$ , we obtain (18). The proof is now complete.

## APPENDIX B

### PROOF OF THEOREM 3

Based on the result derived in (16) and exploiting the fact that the elements of  $\mathbf{Q}_3$  and  $\mathbf{Q}_{v,4}$  are i.n.i.d., the effective channel gain vector of user  $m$  (eavesdropper) can be transformed into

$$\left\| \hat{\mathbf{h}}_{\chi, \text{LIS}} \right\|_F^2 = \sum_{q=1}^Q \sum_{n=1}^{MN} |(q_{q,n}^{\chi,4}) (q_{n,m}^{u_i,3})|^2 = \sum_{q=1}^Q \sum_{n=1}^{MN} |q_{q,n}^{\chi,4}|^2 |q_{n,m}^{u_i,3}|^2. \quad (\text{B-1})$$

Note that  ${}_{\chi,4}q_{q,n} \sim \mathcal{F}\left(m_{q,n}^{\chi,4}, m_{s_{q,n}}^{\chi,4}, \Omega_{q,n}^{\chi,4}\right)$  and  $q_{n,m}^{u,3} \sim \mathcal{F}\left(m_{n,m}^{u,3}, m_{s_{n,m}}^{u,3}, \Omega_{n,m}^{u,3}\right)$  are i.n.i.d. Fisher-Snedecor  $\mathcal{F}$  RVs. Again, we define that  $\{q_\ell\}_{i=1}^{QMN} = \left\{ \left\{ (q_{q,n}^{\chi,4}) (q_{n,m}^{u,3}) \right\}_{n=1}^{MN} \right\}_{q=1}^Q$  in order to make our proof process more concise.

Thus, using [42, eq. (18)] and letting  $N = 2$  and  $\gamma_\ell = \bar{\gamma}_\ell \frac{|q_\ell|^2}{\Omega_{1,\ell} \Omega_{2,\ell}}$ , the MGF of  $\gamma_\ell$  can be expressed as

$$M_\gamma(\gamma_\ell) = \frac{G_{3,2}^{2,3} \left( \frac{m_{1,\ell} m_{2,\ell}}{(m_{s_{1,\ell}} - 1)(m_{s_{2,\ell}} - 1) \bar{\gamma}_\ell \gamma_\ell} \middle| \begin{matrix} 1, 1 - m_{s_{1,\ell}}, 1 - m_{s_{2,\ell}} \\ m_{1,\ell}, m_{2,\ell} \end{matrix} \right)}{\Gamma(m_{1,\ell}) \Gamma(m_{s_{1,\ell}}) \Gamma(m_{2,\ell}) \Gamma(m_{s_{2,\ell}})}. \quad (\text{B-2})$$

Letting  $X = \sum_{\ell=1}^{QMN} |\gamma_\ell|$ , we can derive the PDF of  $X$  as

$$f_X(x) = \mathcal{L}^{-1} \{ \mathcal{M}_X(s); x \} = \frac{1}{2\pi j} \int_{\mathcal{L}} \mathcal{M}_X(s) e^{xs} ds, \quad (\text{B-3})$$

where  $\mathcal{L}^{-1}\{\cdot\}$  denotes the inverse Laplace transform. The MGF of the  $X$  can be expressed with the aid of (B-2) and [21, eq. (8.4.3.1)]

$$f_X(x) = \frac{1}{2\pi j} \int_{\mathcal{L}} \prod_{\ell=1}^{QMN} \mathcal{M}_{\gamma_\ell}(s) e^{xs} ds = \frac{1}{2\pi j} \int_{\mathcal{L}} \prod_{\ell=1}^{QMN} \frac{1}{\Gamma(m_{1,\ell}) \Gamma(m_{s_{1,\ell}}) \Gamma(m_{2,\ell}) \Gamma(m_{s_{2,\ell}})} \left( \frac{1}{2\pi j} \right)^{QMN} \\ \times \int_{\mathcal{L}_{QMN}} \cdots \int_{\mathcal{L}_1} \Upsilon(\zeta_\ell) \left( \frac{m_{1,\ell} m_{2,\ell}}{(m_{s_{1,\ell}} - 1)(m_{s_{2,\ell}} - 1) \bar{\gamma}_\ell s} \right)^{-\zeta_\ell} d\zeta_1 \cdots d\zeta_{QMN} e^{xs} ds, \quad (\text{B-4})$$

where  $\Upsilon(\zeta_\ell) = \Gamma(-\zeta_\ell) \Gamma(m_{s_{1,\ell}} - \zeta_\ell) \Gamma(m_{s_{2,\ell}} - \zeta_\ell) \Gamma(m_{1,\ell} + \zeta_\ell) \Gamma(m_{2,\ell} + \zeta_\ell)$ . Note that the order of integration can be interchangeable according to Fubini's theorem, we can re-write (B-4) as

$$f_X(x) = \prod_{\ell=1}^{QMN} \frac{1}{\Gamma(m_{1,\ell}) \Gamma(m_{s_{1,\ell}}) \Gamma(m_{2,\ell}) \Gamma(m_{s_{2,\ell}})} \left( \frac{1}{2\pi j} \right)^{QMN} \\ \times \int_{\mathcal{L}_{QMN}} \cdots \int_{\mathcal{L}_1} \Upsilon(\zeta_\ell) \left( \frac{m_{1,\ell} m_{2,\ell}}{(m_{s_{1,\ell}} - 1)(m_{s_{2,\ell}} - 1) \bar{\gamma}_\ell} \right)^{-\zeta_\ell} \underbrace{\frac{1}{2\pi j} \int_{\mathcal{L}} s^{\sum_{\ell=1}^{QMN} \zeta_\ell} e^{xs} ds}_{I_{B_1}} d\zeta_1 \cdots d\zeta_{QMN}. \quad (\text{B-5})$$

Letting  $xs = -t$  and using [21, eq. (8.315.1)], we can derive  $I_{B_1}$  as

$$I_{B_1} = \frac{x^{-1 - \sum_{\ell=1}^{QMN} \zeta_\ell}}{\Gamma\left(-\sum_{\ell=1}^{QMN} \zeta_\ell\right)}. \quad (\text{B-6})$$

Substituting (B-6) into (B-5), we obtain the PDF of  $X$ , which can be written as Fox's  $H$  function. The

CDF of  $X$  can be expressed as

$$F_X(x) = \int_0^x f_r(r) dr. \quad (\text{B-7})$$

Thus, we can rewrite the CDF of  $X$  as

$$F_X(x) = \prod_{\ell=1}^{QMN} \frac{1}{\Gamma(m_{1,\ell}) \Gamma(m_{s_{1,\ell}}) \Gamma(m_{2,\ell}) \Gamma(m_{s_{2,\ell}})} \left(\frac{1}{2\pi j}\right)^{QMN} \\ \times \int_{\mathcal{L}_{QMN}} \cdots \int_{\mathcal{L}_1} \frac{\Upsilon(\zeta_\ell)}{\Gamma\left(-\sum_{\ell=1}^L \zeta_\ell\right)} \left(\frac{m_{1,\ell} m_{2,\ell}}{(m_{s_{1,\ell}} - 1)(m_{s_{2,\ell}} - 1) \bar{\gamma}_\ell}\right)^{-\zeta_\ell} \underbrace{\int_0^x r^{-1 - \sum_{\ell=1}^{QMN} \zeta_\ell} dr}_{I_{B_2}} d\zeta_1 \cdots d\zeta_{QMN}, \quad (\text{B-8})$$

where  $I_{B_2}$  can be solved as

$$I_{B_2} = \int_0^x r^{-1 - \sum_{\ell=1}^{QMN} \zeta_\ell} dr = \frac{1}{-\sum_{\ell=1}^{QMN} \zeta_\ell} x^{-\sum_{\ell=1}^{QMN} \zeta_\ell}. \quad (\text{B-9})$$

Substituting (B-9) into (B-8) and using [21, eq. (8.331.1)], equation (B-8) can be expressed as

$$F_X(x) = \prod_{\ell=1}^{QMN} \frac{1}{\Gamma(m_{1,\ell}) \Gamma(m_{s_{1,\ell}}) \Gamma(m_{2,\ell}) \Gamma(m_{s_{2,\ell}})} \left(\frac{1}{2\pi j}\right)^{QMN} \\ \times \int_{\mathcal{L}_{QMN}} \cdots \int_{\mathcal{L}_1} \frac{\Upsilon(\zeta_\ell)}{\Gamma\left(1 - \sum_{\ell=1}^L \zeta_\ell\right)} \left(\frac{x m_{1,\ell} m_{2,\ell}}{(m_{s_{1,\ell}} - 1)(m_{s_{2,\ell}} - 1) \bar{\gamma}_\ell}\right)^{-\zeta_\ell} d\zeta_1 \cdots d\zeta_{QMN}. \quad (\text{B-10})$$

In order to avoid complex trigonometric operations, we assume that  $d_{\chi,\sigma}$  and  $d_{\chi,4}$  are i.n.i.d. RVs. To verify that this assumption will only cause small errors for our considered system, we perform Monte-Carlo simulation for the location of user  $m$  with  $r_0 = 1$ . In the simulation, we generate the location of user  $m$  for  $1e6$  times according to [29, eq. (30)]. Fig. 7 shows that when the distance from the LIS to the BS, defined as  $r_{\text{LIS}}$ , and the range of the system model,  $r_2$ , change, the difference between the mean distance from user  $m$  to the BS and to the LIS is very small. For example, the maximum is less than 5 meters.

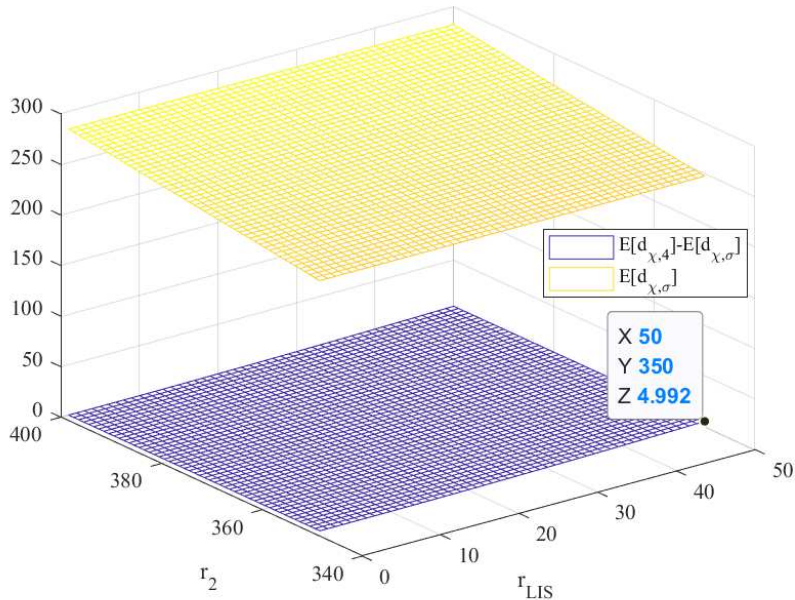


Fig. 7. The difference between the expected distance from the user to the BS and the expected distance from the user to the LIS.

Thus, let  $Y = X/D$ , hence, we can derive the CDF of  $Y$  using (A-5)

$$F_Y(y) = \frac{2}{(r_2^2 - r_0^2) \alpha} \prod_{\ell=1}^{QMN} \frac{1}{\Gamma(m_{1,\ell}) \Gamma(m_{s_{1,\ell}}) \Gamma(m_{2,\ell}) \Gamma(m_{s_{2,\ell}})} \left( \frac{1}{2\pi j} \right)^{QMN} \\ \times \int_{\mathcal{L}_{QMN}} \dots \int_{\mathcal{L}_1} \frac{\Upsilon(\zeta_\ell)}{\Gamma\left(1 - \sum_{\ell=1}^L \zeta_\ell\right)} \left( \frac{xm_{1,\ell}m_{2,\ell}}{(m_{s_{1,\ell}} - 1)(m_{s_{2,\ell}} - 1)\bar{\gamma}_\ell} \right)^{-\zeta_\ell} \underbrace{\int_{r_0^\alpha}^{r_2^\alpha} y^{\frac{2}{\alpha}-1-\sum_{\ell=1}^L \zeta_\ell} dy}_{I_{B_3}} d\zeta_1 \dots d\zeta_{QMN}. \quad (\text{B-11})$$

$I_{B_3}$  can be solved easily. Let  $\alpha = 2$  and  $Z = A_2 Y$ , we obtain (23) and complete the proof.

## REFERENCES

- [1] T. J. Cui, M. Q. Qi, X. Wan, J. Zhao, and Q. Cheng, "Coding metamaterials, digital metamaterials and programmable metamaterials," *Light: Science & Applications*, vol. 3, no. 10, p. 218, Oct. 2014.
- [2] Q. Wu and R. Zhang, "Intelligent reflecting surface enhanced wireless network via joint active and passive beamforming," *IEEE Trans. Wireless Commun.*, vol. 18, no. 11, pp. 5394–5409, Aug. 2019.
- [3] C. Huang, A. Zappone, G. C. Alexandropoulos, M. Debbah, and C. Yuen, "Reconfigurable intelligent surfaces for energy efficiency in wireless communication," *IEEE Trans. Wireless Commun.*, vol. 18, no. 8, pp. 4157–4170, Aug. 2019.
- [4] Q.-U.-A. Nadeem, A. Kammoun, A. Chaaban, M. Debbah, and M.-S. Alouini, "Large intelligent surface assisted MIMO communications," *arXiv:1903.08127*, 2019.
- [5] X. Chen, D. W. K. Ng, W. H. Gerstacker, and H.-H. Chen, "A survey on multiple-antenna techniques for physical layer security," *IEEE Commun. Surveys Tuts.*, vol. 19, no. 2, pp. 1027–1053, Feb. 2016.
- [6] A. D. Wyner, "The wire-tap channel," *Bell Syst. Tech. J.*, vol. 54, no. 8, pp. 1355–1387, 1975.

- [7] H. Du, J. Zhang, K. P. Peppas, H. Zhao, B. Ai, and X. Zhang, "On the distribution of the ratio of products of Fisher-Snedecor  $\mathcal{F}$  random variables and its applications," *IEEE Trans. Veh. Technol.*, vol. 69, no. 2, pp. 1855–1866, Feb. 2020.
- [8] H.-M. Wang, T.-X. Zheng, J. Yuan, D. Towsley, and M. H. Lee, "Physical layer security in heterogeneous cellular networks," *IEEE Trans. Commun.*, vol. 64, no. 3, pp. 1204–1219, Mar. 2016.
- [9] Y.-W. P. Hong, P.-C. Lan, and C.-C. J. Kuo, "Enhancing physical-layer secrecy in multiantenna wireless systems: An overview of signal processing approaches," *IEEE Signal Processing Mag.*, vol. 30, no. 5, pp. 29–40, May 2013.
- [10] S. Goel and R. Negi, "Guaranteeing secrecy using artificial noise," *IEEE Trans. Wireless Commun.*, vol. 7, no. 6, pp. 2180–2189, Jun. 2008.
- [11] T.-X. Zheng, H.-M. Wang, and Q. Yin, "On transmission secrecy outage of a multi-antenna system with randomly located eavesdroppers," *IEEE Commun. Lett.*, vol. 18, no. 8, pp. 1299–1302, Aug. 2014.
- [12] G. Geraci, H. S. Dhillon, J. G. Andrews, J. Yuan, and I. B. Collings, "Physical layer security in downlink multi-antenna cellular networks," *IEEE Trans. Commun.*, vol. 62, no. 6, pp. 2006–2021, Jun. 2014.
- [13] H.-M. Wang, C. Wang, D. W. K. Ng, M. H. Lee, and J. Xiao, "Artificial noise assisted secure transmission for distributed antenna systems," *IEEE Trans. on Signal Processing*, vol. 64, no. 15, pp. 4050–4064, Apr. 2016.
- [14] X. Zhou, R. K. Ganti, and J. G. Andrews, "Secure wireless network connectivity with multi-antenna transmission," *IEEE Trans. Wireless Commun.*, vol. 10, no. 2, pp. 425–430, Feb. 2010.
- [15] X. Yu, D. Xu, and R. Schober, "Enabling secure wireless communications via intelligent reflecting surfaces," *arXiv:1904.09573*, 2019.
- [16] M. Cui, G. Zhang, and R. Zhang, "Secure wireless communication via intelligent reflecting surface," *IEEE Wireless Commun. Lett.*, to appear, 2019.
- [17] J. Chen, Y.-C. Liang, Y. Pei, and H. Guo, "Intelligent reflecting surface: A programmable wireless environment for physical layer security," *arXiv:1905.03689*, 2019.
- [18] S. N. Chiu, D. Stoyan, W. S. Kendall, and J. Mecke, *Stochastic geometry and its applications*. John Wiley & Sons, 2013.
- [19] M. Haenggi, *Stochastic geometry for wireless networks*. Cambridge University Press, 2012.
- [20] H. Du, J. Zhang, K. P. Peppas, H. Zhao, B. Ai, and X. Zhang, "Sum of Fisher-Snedecor  $\mathcal{F}$  random variables and its applications," *IEEE Open J. Commun. Soc.*, to appear, Mar. 2020.
- [21] I. S. Gradshteyn and I. M. Ryzhik, *Table of integrals, Series, and Products*, 7th ed. Academic Press, 2007.
- [22] Q.-U.-A. Nadeem, A. Kammoun, A. Chaaban, M. Debbah, and M.-S. Alouini, "Intelligent reflecting surface assisted wireless communication: Modeling and channel estimation," 2019.
- [23] Z. Wang, L. Liu, and S. Cui, "Channel estimation for intelligent reflecting surface assisted multiuser communications: Framework, algorithms, and analysis," *arXiv preprint arXiv:1912.11783*, 2019.
- [24] A. Mukherjee, S. A. A. Fakoorian, J. Huang, and A. L. Swindlehurst, "Principles of physical layer security in multiuser wireless networks: A survey," *IEEE Commun. Surveys Tuts.*, vol. 16, no. 3, pp. 1550–1573, Mar. 2014.
- [25] M. Haenggi, J. G. Andrews, F. Baccelli, O. Dousse, and M. Franceschetti, "Stochastic geometry and random graphs for the analysis and design of wireless networks," *IEEE J. Sel. Areas Commun.*, vol. 27, no. 7, pp. 1029–1046, July 2009.
- [26] S. Singh, M. N. Kulkarni, A. Ghosh, and J. G. Andrews, "Tractable model for rate in self-backhauled millimeter wave cellular networks," *IEEE J. Sel. Areas Commun.*, vol. 33, no. 10, pp. 2196–2211, Oct. 2015.
- [27] M. Di Renzo, "Stochastic geometry modeling and analysis of multi-tier millimeter wave cellular networks," *IEEE Trans. Wireless Commun.*, vol. 14, no. 9, pp. 5038–5057, Sept. 2015.
- [28] T. Bai and R. W. Heath, "Coverage and rate analysis for millimeter-wave cellular networks," *IEEE Trans. Wireless Commun.*, vol. 14, no. 2, pp. 1100–1114, Feb. 2014.

- [29] T. Hou, Y. Liu, Z. Song, X. Sun, Y. Chen, and L. Hanzo, "MIMO assisted networks relying on large intelligent surfaces: A stochastic geometry model," *arXiv:1910.00959*, Oct. 2019.
- [30] M. R. Akdeniz, Y. Liu, M. K. Samimi, S. Sun, S. Rangan, T. S. Rappaport, and E. Erkip, "Millimeter wave channel modeling and cellular capacity evaluation," *IEEE J. Sel. Areas Commun.*, vol. 32, no. 6, pp. 1164–1179, Jun. 2014.
- [31] W. Tang, M. Z. Chen, X. Chen, J. Y. Dai, Y. Han, M. Di Renzo, Y. Zeng, S. Jin, Q. Cheng, and T. J. Cui, "Wireless communications with reconfigurable intelligent surface: Path loss modeling and experimental measurement," *arXiv:1911.05326*, Nov. 2019.
- [32] S. K. Yoo, P. C. Sofotasios, S. L. Cotton, S. Muhaidat, F. J. Lopez-Martinez, J. M. Romero-Jerez, and G. K. Karagiannidis, "A comprehensive analysis of the achievable channel capacity in  $\mathcal{F}$  composite fading channels," *IEEE Access*, vol. 7, pp. 34 078 –34 094, Mar 2019.
- [33] J. Wang, L. Kong, and M.-Y. Wu, "Capacity of wireless ad hoc networks using practical directional antennas," in *Proc. IEEE WCNC*, 2010, pp. 1–6.
- [34] X. Yu, D. Xu, and R. Schober, "Optimal beamforming for MISO communications via intelligent reflecting surfaces," *arXiv preprint arXiv:2001.11429*, 2020.
- [35] A. M. Elbir, A. Papazafeiropoulos, P. Kourtessis, and S. Chatzinotas, "Deep channel learning for large intelligent surfaces aided mmWave massive MIMO systems," *arXiv preprint arXiv:2001.11085*, 2020.
- [36] H. Du, J. Zhang, J. Cheng, Z. Lu, and B. Ai, "Millimeter wave communications with reconfigurable intelligent surface: Performance analysis and optimization," *arXiv preprint arXiv:2003.09090*, 2020.
- [37] A. M. Mathai, R. K. Saxena, and H. J. Haubold, *The H-function: Theory and Applications*. Springer Science & Business Media, 2009.
- [38] Y. A. Rahama, M. H. Ismail, and M. S. Hassan, "On the sum of independent Fox's  $H$  -function variates with applications," *IEEE Trans. Veh. Technol.*, vol. 67, no. 8, pp. 6752–6760, Aug. 2018.
- [39] L. Kong and G. Kaddoum, "On physical layer security over the Fisher-Snedecor  $\mathcal{F}$  wiretap fading channels," *IEEE Access*, vol. 6, pp. 39 466–39 472, Jun. 2018.
- [40] M. Bloch, J. Barros, M. R. Rodrigues, and S. W. McLaughlin, "Wireless information-theoretic security," *IEEE Trans. Inf. Theory*, vol. 54, no. 6, pp. 2515–2534, Jun. 2008.
- [41] Wolfram, "The wolfram functions site," <http://functions.wolfram.com>.
- [42] O. S. Badarneh, S. Muhaidat, P. C. Sofotasios, S. L. Cotton, K. Rabie, and D. B. da Costa, "The  $N^*$ Fisher-Snedecor  $\mathcal{F}$  cascaded fading model," in *Proc. IEEE WiMbo*, Oct. 2018, pp. 1–7.